Compared performances of SMOS-IC soil moisture and vegetation optical depth retrievals based on Tau-Omega and Two-Stream microwave emission models

Xiaojun Li, Amen Al-Yaari, Mike Schwank, Lei Fan, Frédéric Frappart, Jennifer Swenson, Jean-Pierre Wigneron

Compared performances of SMOS-IC soil moisture and vegetation optical depth retrievals based on Tau-Omega and Two-Stream microwave emission models.

X. Li[a], A. Al-Yaari[a], M. Schwank[b,c], Lei Fan[d,a], F. Frappart[e,a], J. Swenson[f,a], J.-P. Wigneron[a*]

[a] INRA, UMR1391 ISPA, F-33140 Villenave d'Ornon, France

[b] Swiss Federal Research Institute WSL, CH-8903 Birmensdorf, Switzerland

[c] Gamma Remote Sensing AG, CH-3073 Gümligen, Switzerland

[d] Collaborative Innovation Center on Forecast and Evaluation of Meteorological Disaster, School of Geographical Sciences, Nanjing University of Information Science and Technology, Nanjing 210044, China

[e] Laboratoire d'Etudes en Géophysique et Océanographie Spatiales (LEGOS), 31400 Toulouse, France

[f] Nicholas School of the Environment, Duke University, Durham, NC 27708, USA

[*]Corresponding Author: J.-P. Wigneron (jean-pierre.wigneron@inra.fr)

Abstract

Since 2010, SMOS (Soil Moisture and Ocean Salinity) retrievals of surface soil moisture (SM) and vegetation optical depth (VOD) have been produced through the inversion of the so-called Tau-Omega (TO) vegetation emission model. Tau-Omega is a 0^{th}-order solution of the radiative transfer equations that neglects multiple scattering, conversely to 1^{st}-order solutions as Two-Stream (2S). To date, very little is known about the compared retrieval performances of these emission models. Here, we inter-compared (SM, VOD) retrievals using the SMOS-IC algorithm running with the TO and 2S emission models. Retrieval performances obtained from TO and 2S were found to be relatively similar, except that a larger dry bias and a slightly lower SM unbiased RMSD were obtained with 2S and the VOD values of the two models vary over dense vegetation areas, both in terms of magnitude and seasonal variations. Considering this and the enhanced physical background of 2S that allows its implementation as a unified emission model for

different applications, our study reveals the high interest of using Two-Stream in global retrieval algorithms at L-band.

Key words: Microwave emission model, SMOS-IC, Tau-Omega, Two-Stream, Soil moisture, Vegetation optical depth, global retrievals, biomass, ECMWF, MODIS NDVI, ISMN

1. Introduction

Surface Soil Moisture (SM) is a key state variable in the climate and environment system as it strongly impacts the energy and water balance at the land-surface/atmosphere interface (Koster et al., 2004; Taylor et al., 2011). It also plays a key role for a wide range of hydrological applications (Laiolo et al., 2016; Wagner et al., 2007), agriculture applications (Roy et al., 2016), weather predictions (Tuttle and Salvucci, 2016), and carbon cycle (Jung et al., 2017).

Passive L-band microwave remote sensing with frequent revisits is recognized as a promising tool for mapping the regional and global SM distribution (Entekhabi et al., 2010; Kerr et al., 2010; Jackson et al., 2010). Operational space missions using this technology include Soil Moisture and Ocean Salinity (SMOS), the first mission dedicated specifically to SM mapping, launched in 2009 by the European space agency (ESA) (Kerr et al., 2010; Kerr et al., 2001) and Soil Moisture Active Passive (SMAP), the most recent space-borne L-band mission, launched in 2015 by the National Aeronautics and Space Administration (NASA) (Entekhabi et al., 2010).

The operational SMOS retrieval algorithm relies on the dual-polarization and multi-angular capabilities of the SMOS synthetic aperture radiometer (Wigneron et al., 2017). SM and vegetation optical depth (VOD), a parameter characterizing vegetation extinction effects, are produced simultaneously from the inversion of the L-band Microwave Emission of the Biosphere model (L-MEB; Wigneron et al., 2000). SMOS VOD, as a potentially useful ecological indicator, has been widely used for vegetation seasonality (Tian et al., 2018), crop modelling (Chaparro et

al., 2018; Hornbuckle et al., 2016), and biomass estimation (Brandt et al., 2018; Fan et al., 2019b). In the recently developed SMOS-IC algorithm, VOD and SM are retrieved without external vegetation or hydrologic products as inputs to the L-MEB forward emission model, making the SMOS-IC product very interesting for robust applications and inter-comparison analyses (Al-Yaari et al., 2019b). The current retrieval algorithm of the official SMAP SM product is based on the Single Channel Algorithm (SCA) (Jackson, 1993) that only retrieves SM, while VOD is estimated from a linear relationship with vegetation water content (VWC) (O'Neill et al., 2015). Recently, Konings et al. (2017) have developed a multi-temporal dual-channel retrieval algorithm (MT-DCA) to simultaneously retrieve SM and VOD from the mono-angular SMAP observations.

Currently, both SMAP and SMOS releases of the SM and VOD products are based on the inversion of the Tau-Omega emission model (referred to as TO or Tau-Omega in the following) (Mo et al., 1982). Tau-Omega includes radiative transfer contributions from the soil surface and the vegetation canopy represented by a uniform "soft layer", *e.g.* refraction and reflection at its upper bound are ignored. As a 0^{th}-order solution (the scattering phase function is set to zero) of the radiative transfer (RT) equations, Tau-Omega neglects multiple reflections at the soil-vegetation interface, and it is also incompatible with Kirchhoff's law (Mätzler, 2000). Furthermore, by neglecting multiple scattering effects within the vegetation layer, Tau-Omega provides an insufficient representation of volume scattering effects in dense vegetation (Feldman et al., 2018). However, Kurum (2013) has found that by considering volume scattering through an equivalent scattering albedo, the 1^{st}-order solution of the RT equations can be well represented by the 0^{th}-order Tau-Omega. Such an approach was used by Ferrazzoli et al. (2002) to represent scattering effects over forests.

In contrast to Tau-Omega, higher order solutions of the RT equations have been proposed (Feldman et al., 2018; Schwank et al., 2018). Among them, the Two-Stream emission model (referred to as 2S in the following), was developed in the context of the "Microwave Emission Model of Layered Snowpacks" (MEMLS) (Mätzler, 1998; Wiesmann and Mätzler, 1999). 2S holds a stronger physical background than Tau-Omega; in particular, it considers multiple scattering and reflection. Furthermore, the "soft layer" assumption (*e.g.* neglecting refraction and reflection at the upper interface of the medium) is not required in 2S. The latter advantage is crucial to represent brightness temperatures (TB) over snow-covered ground (Schwank et al., 2018; Lemmetyinen et al., 2016). The single-layer configuration of the L-band Specific Microwave Emission Model of Layered Snowpacks (LS-MEMLS), which includes 2S, has been used to estimate snow liquid water content (Derek et al, submitted; Naderpour and Schwank, 2018; Naderpour et al., 2017) and snow density (Lemmetyinen et al., 2016; Schwank et al., 2015; Schwank and Naderpour, 2018) from L-band radiometry.

To summarize, in theory, using 2S instead of Tau-Omega in retrieving SM and VOD at global scale presents almost only some advantages. Using 2S would allow:

(i) the development of retrieval algorithms with the same microwave emission model (EM) to estimate SM and VOD (Konings et al., 2017; Wigneron et al., 2007, 2017), snow properties (Naderpour and Schwank, 2018; Schwank and Naderpour, 2018; Lemmetyinen et al., 2016; Schwank et al., 2015), and ground freeze or thaw conditions (Derksen et al., 2017; Rautiainen et al., 2014). This development would be thus a key step in simplifying global retrieval algorithms. Because, presently the use of distinct models (Tau-Omega to retrieve SM and VOD or 2S to retrieve snow properties and ground freeze or thaw conditions), requires the use of a decision tree and of ancillary data to detect what is the soil surface status (frozen or non-frozen soil conditions?

96 snow presence? etc.). All this makes global retrievals more complex. The use of a single model
97 (2S) for all surface conditions would make the retrieval algorithm much simpler and would be
98 thus crucial for achieving full exploitation of satellite-based passive L-band observations.

99 (ii) the use of first order solution of the RT equations, which theoretically provides a better
100 representation of volume scattering effects in dense vegetation. This is potentially a key step to
101 achieve accurate SM and VOD retrievals in dense forests, especially in the Amazon and Congo
102 basins, which are key vegetation areas of the global water and carbon cycle (Fan et al., 2019b).

103 (iii) using a first order solution of the RT equations which is very simple (the formulation of
104 the single layer 2S is almost as simple as that of the Tau-Omega model (Schwank et al., 2019))
105 and which can be easily substituted to the Tau-Omega model, using transformation equations for
106 the vegetation scattering parameter as developed by Schwank et al. 2018 (see Appendix).

107 So using 2S in global operational algorithms of the SMOS and SMAP missions is very
108 promising. However, the application of 2S to achieve global SM and VOD retrievals from
109 satellite measurements requires an accurate and large-scale evaluation which has not been yet
110 carried out. Schwank et al. (2018) have compared the performance of 2S and Tau-Omega in
111 simulating TB and retrieving SM and VOD based on synthetic and close-distance (tower-based)
112 L-band TB measured during the "Forest Soil Moisture Experiment" (FOSMEX) (Guglielmetti et
113 al., 2008). But, as most evaluation studies of 2S have been made to date at a local scale, it is not
114 possible to confirm that 2S is an accurate model for global retrievals of SM and VOD. The
115 objective of this study is address this issue and to investigate the performance of 2S for retrieving
116 global SM and VOD in comparison to corresponding retrievals achieved with the traditional Tau-
117 Omega model using the SMOS-IC retrieval algorithm (Fernandez-Moran et al., 2017a; Wigneron

et al., 2018). In this study, the current SMOS-IC algorithm version V105 was either used in its traditional Tau-Omega retrieval configuration (SMOS-IC_{TO}) or in the 2S configuration (SMOS-IC_{2S}). Soil moisture retrievals SM_{EM} achieved with emission models EM = TO or EM = 2S were inter-compared against the "European Centre for Medium-Range Weather Forecasts" (ECMWF) modelled SM and the "International Soil Moisture Network" (ISMN) (Dorigo et al., 2015; Dorigo et al., 2017) *in-situ* measurements during 2011 – 2017. Retrievals of VOD_{2S} and VOD_{TO} were compared to the "Normalized Difference Vegetation Index" (NDVI) and above-ground biomass (AGB) (Saatchi et al., 2011). Note that the present study used exclusively SMOS data, but the final implications are not only relevant for SMOS, but also for other passive L-band missions (e.g., SMAP).

2. Materials and methods

2.1. Datasets

2.1.1. SMOS TB products

One input of the SMOS-IC retrieval algorithm is SMOS-Level3 (L3) brightness temperatures (TB) generated and delivered by CATDS (Centre Aval de Traitements des Données SMOS). The daily SMOS-L3 TB product consists of brightness temperatures $T_B^{p,\theta}$ measured at horizontal and vertical polarizations ($p = \{H, V\}$) and multiple observation angles θ relative to nadir. SMOS-L3 TB are available for both descending and ascending orbits and are projected on a global Equal Area Scalable Earth Grid version 2 (EASE-Grid 2.0), with a spatial resolution of 25 km (Al Bitar et al., 2017). SMOS-L3 TB are top of the atmosphere observations (Al-Yaari et al., 2017) and are averaged in observation angle bins of 5°, with a bin center ranging from 2.5° to 62.5°. In this study, only TB (θ) layers with $20° \leq \theta \leq 55°$ and a range of available angular values larger than

10° (Fernandez-Moran et al., 2017a; Fernandez-Moran et al., 2017b) were used, since the error in SM retrievals decreases for increasing ranges of incidence angles (Wigneron et al., 2000).

2.1.2. SMOS-IC SM and VOD products

We used the current SMOS-IC algorithm version V105, which is an alternative to the SMOS-L2 and SMOS-L3 algorithms (Fernandez-Moran et al., 2017a), to perform the SM and VOD retrievals. SMOS-IC was used here because it is simple and it is independent of auxiliary variables making it very robust for testing (Wigneron et al., 2018) and applications (Al-Yaari et al., 2019a; Brandt et al., 2018; Tian et al., 2018). The SMOS-IC VOD product has been shown to perform very well relatively to other SMOS products when compared to reference datasets such as above ground biomass, tree height and mean annual precipitation, etc. (Rodríguez-Fernández et al., 2018). Moreover, recent SM inter-comparison studies with other remotely-sensed products (ASCAT H111, CCI V04.2, SMOSL2 V650, SMOSL3 V300, and SMAPL3 V4) have shown that SMOS-IC also performs very well and with similar accuracy as SMAP SM (Al-Yaari et al., 2019b; Colliander et al., 2019; Quets et al., in press).

The SMOS-IC algorithm relies on a 2-Parameter (i.e., SM and VOD) inversion of the L-MEB model as defined in Wigneron et al. (2000, 2007). In the L-MEB approach, the 0^{th}-order Tau-Omega emission model (Mo et al., 1982) is used and the 2-Parameter retrieval of SM and VOD is achieved by minimizing a cost function that includes the root mean square difference between observed and simulated TB. We refer readers to Wigneron et al. (2000, 2007, 2017) for more details on the L-MEB forward emission model. The main features of SMOS-IC are given below:

1) Through an efficient use of the TB data from multiple observation angles, the SMOS-IC retrieval algorithm is designed to be as independent as possible from auxiliary data. Notably,

ECMWF modeled soil moisture or Moderate Resolution Imaging Spectroradiometer (MODIS) Leaf Area Index (LAI) products are not used in SMOS-IC over heterogeneous pixels including forests (Al-Yaari et al., 2019b). This minimal use of auxiliary data makes SMOS-IC well-suited and robust for a wide range of applications in the field of hydrology and large scale vegetation monitoring.

2) SMOS-IC is much simpler than the SMOS-L2 and SMOS-L3 algorithms. For instance, SMOS-IC does not attempt to characterize the effects of antenna patterns varying with view angle and azimuth. It also considers pixels as homogeneous to reduce the use of auxiliary datasets characterizing the pixel heterogeneity (Ebrahimi-Khusfi et al., 2018; Fernandez-Moran et al., 2017a).

3) Model parameters used to represent effects of soil roughness (Lawrence et al., 2013) and vegetation have been recently optimized (Fernandez-Moran et al., 2017b). The so-called H_R roughness parameter was estimated from the global roughness map of Parrens et al. (2016).

The SMOS-IC SM product is currently available online via CATDS in the Network Common Data Form (NetCDF) format for both orbits on a global EASE-Grid 2.0, with a sampling resolution of 25 km.

2.1.3. ECMWF data

In this study, we used the ECMWF modelled soil temperatures and SM datasets (top 0–7 cm soil layer; referred to as SM_{ECMWF} in the following). The ECMWF product is derived from the ERA-Interim dataset, which is based on IFS-Cy31r2 (a numerical weather prediction (NWP) system) to solve for parameters including different layer volumetric soil moisture (Berrisford et al., 2011). Details about this ERA-Interim modelling and the data assimilation system can be

185 referred to (Berrisford et al., 2011; Dee et al., 2011). ECMWF modelled soil temperatures were
186 used to calculate effective soil temperatures T_s for the SMOS-IC algorithm based on the
187 formulation of Wigneron et al. (2001). The SMOS-IC SM retrievals were compared to SM_{ECMWF}
188 at global scale. The ECMWF dataset was resampled using the SMOS-L3 pre-processor to be in
189 the same format (i.e., EASE-Grid 2.0). SM_{ECMWF} has been shown to represent well the SM
190 variability at global scale (Albergel et al., 2012; Fernandez-Moran et al., 2017a).

191 ### *2.1.4. ISMN ground-based measurements*

192 SMOS-IC SM retrievals were also evaluated at local scale against *in-situ* SM data (referred
193 to as $SM_{in\text{-}situ}$ in the following) obtained from the ISMN data set (Dorigo et al., 2011). ISMN is an
194 international initiative of GEWEX (Global Energy and Water Cycle Experiment) and ESA,
195 aiming at establishing and maintaining a global *in-situ* soil moisture database (Dorigo et al.,
196 2013). This database aims at promoting scientific studies on the validation and improvement of
197 global satellite observations and land surface modeling. The ISMN database hosts currently SM
198 data from about ~60 networks (products are available at https://ismn.geo.tuwien.ac.at/). In this
199 study, only *in-situ* ISMN networks with sufficiently long time series of SM data covering the
200 period 2011 - 2017 were used. Only SM observations of the top 0~5 cm soil layer with a flag set
201 to "Good" were used (Al-Yaari et al., 2019b; Dorigo et al., 2013). Consequently, 748 sites from
202 27 networks (Table 1) over the USA, Canada, Australia, and Europe were used. Fig. 1 presents
203 the spatial distribution of the *in-situ* sites with the International Geosphere-Biosphere Programme
204 (IGBP) land cover classification shown in the background.

205 **Table 1** *In situ* Networks from ISMN. The type of the land cover is determined by IGBP. Note
206 that a total of 27 networks was used; here we only list the networks with more than 5 available
207 sites, and more data can be viewed in Table S1 in the supplementary materials.

Network name	Country	Number of available	Land cover type	References

		sites		
AMMA-CATCH	Benin, Niger, Mali	6	savannas, cropland/natural vegetation mosaic	Lebel et al. (2009)
ARM	USA	16	grasslands, croplands	https://www.arm.gov/
FMI	Finland	6	woody savannas	Rautiainen et al. (2012)
HOBE	Denmark	28	croplands	http://www.hobe.dk/index.php/soil-moisture-network
OZNET	Australia	8	grasslands, croplands	Smith et al. (2012)
PBO-H2O	USA	54	grasslands, open shrublands, croplands, barren or sparsely vegetated	Larson et al. (2008)
REMEDHUS	Spain	21	croplands	Sanchez et al. (2012)
RISMA	Canada	19	croplands, cropland/natural vegetation mosaic	http://agriculture.canada.ca/SoilMonitoringStations
RSMN	Romania	15	croplands, cropland/natural vegetation mosaic	http://assimo.meteoromania.ro/
SCAN	USA	147	cropland/natural vegetation mosaic, barren or sparsely vegetated, croplands, deciduous broadleaf forest, evergreen needleleaf forest, grasslands, mixed forest, woody savannas, open shrublands	Schaefer et al. (2007)
SMOSMANIA	France	20	croplands, evergreen needleleaf forest, woody savannas, mixed forest, cropland/natural vegetation mosaic	Albergel et al. (2008),Calvet et al. (2007)
SNOTEL	USA	172	croplands, evergreen needleleaf forest, grasslands, woody savannas, open shrublands	Serreze et al. (2001)
SOILSCAPE	USA	117	grasslands, open shrublands, savannas, woody savannas	Moghaddam et al. (2010)
USCRN	USA	88	cropland/natural vegetation mosaic, barren or sparsely vegetated, croplands, deciduous broadleaf forest, evergreen needleleaf forest, grasslands, mixed forest, woody savannas, open shrublands	Bell et al. (2013)

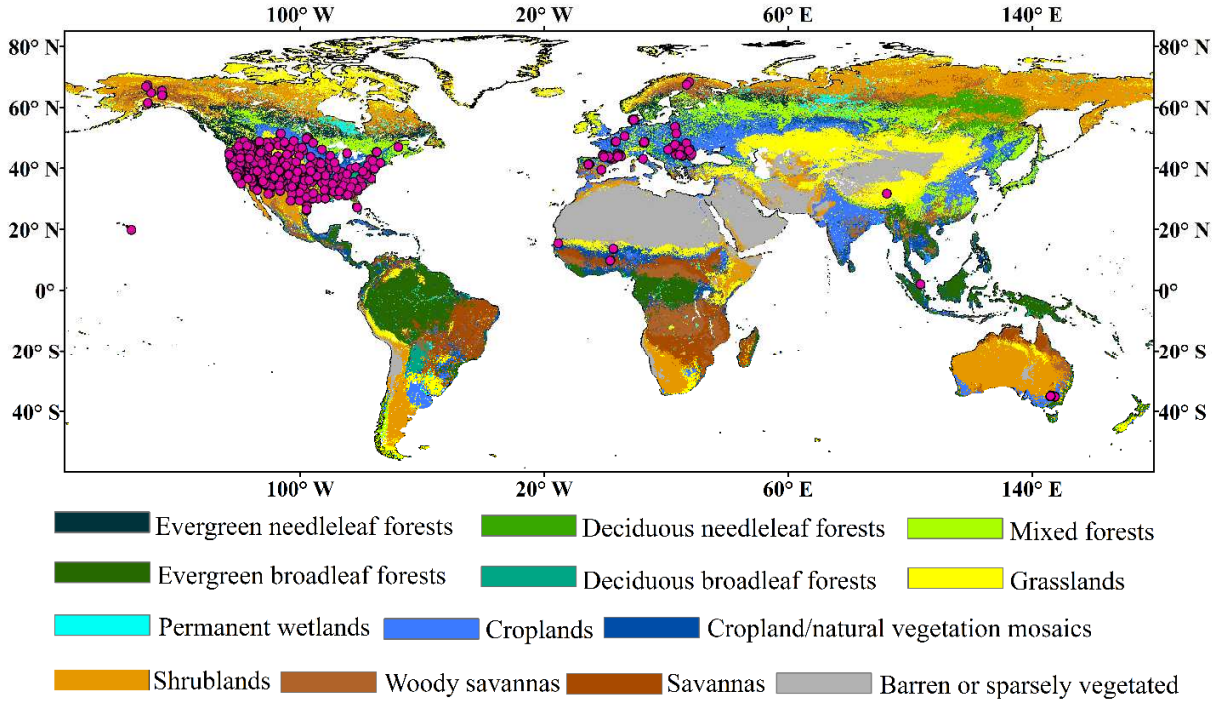

Fig. 1. Spatial distribution of the different *in-situ* sites (pink circles). The IGBP land cover classification is represented in the background.

2.1.5. Additional datasets

Several additional datasets shown in Table 2 were used to interpret the results, including the IGBP land cover classification scheme, MODIS LAI, MODIS NDVI and above-ground biomass (AGB) map. Earlier studies (e.g., Al-Yaari et al., 2019b; Al-Yaari et al., 2014a; Al-Yaari et al., 2014b) have shown that the performance of the remotely-sensed SM retrievals may vary as a function of vegetation density and land cover type. Here, we used the IGBP land cover classification scheme and LAI data (see Fig.2) to account for the different land cover types and vegetation conditions when comparing the SM retrievals. The NDVI and AGB data were intercompared with the SMOS-IC VOD retrievals for both Tau-Omega and 2S configurations at

global scale. All the additional datasets were rescaled to the SMOS-L3 TB resolution, to ensure that all data have the same spatial resolution of 25 km.

Table 2 Additional datasets.

Additional datasets	Spatial resolution	Temporal series	References
IGBP land cover type	500 m	2001 – 2010	Broxton et al. (2014); Fernandez-Moran et al. (2017a)
MODIS LAI (MOD15A2)	0.1 degree	2011 – 2016	https://neo.sci.gsfc.nasa.gov/
MODIS NDVI (MOD13A2)	1 km	2011 – 2017	https://neo.sci.gsfc.nasa.gov/
AGB map	1 km	2015	Saatchi et al. (2011)

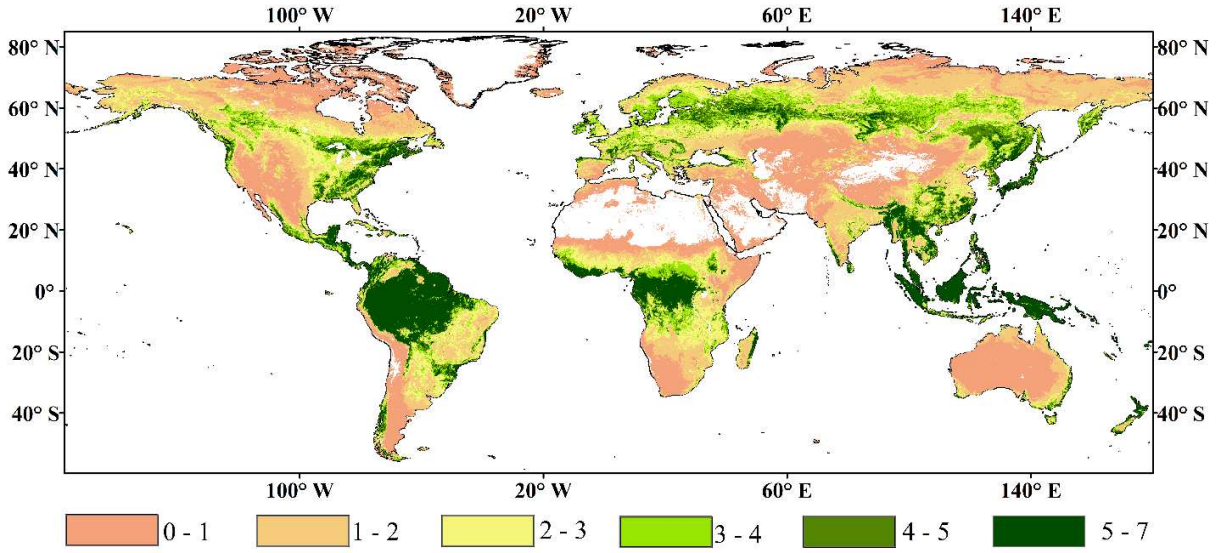

Fig. 2. Global LAI map obtained from MODIS using the maximum value composite (MVC) method (Holben, 1986) during 2011 – 2016.

2.2. Methods

2.2.1 Tau-Omega and Two-stream emission models

Two different microwave emission models (Tau-Omega and 2S) were implemented in the SMOS-IC$_{EM}$ (with *EM* = TO or *EM* = 2S) retrieval algorithms to achieve respective 2-Parameter retrievals (SM_{EM}, VOD_{EM}) of Soil Moisture (SM) and Vegetation Optical Depth (VOD). Note that in this study both "VOD" and "τ" terms are equivalent; the term "τ" being used most often in radiative transfer equations. The 0th-order Tau-Omega model (TO) (Mo et al., 1982) is used in the

operational SMOS and SMAP retrievals over land surfaces, and it is implemented in the current version V105 of SMOS-IC (Fernandez-Moran et al., 2017a). The 1st-order Two-Stream model (2S) was originally developed as part of the "Microwave Emission Model of Layered Snowpacks" (MEMLS) (Mätzler, 1998; Wiesmann and Mätzler, 1999). The common points to both Tau-Omega and the 2S version used here are i) the parameterization of the soil by means of an infinite homogeneous layer with a rough surface, and ii) the parameterization of the above vegetation by means of a single homogeneous "soft-layer".

Detailed equations of the Tau-Omega and 2S models and of the SMOS-IC algorithm based on these two emission models are given, respectively, in the Supplementary text and in the Appendix. Note that to ensure that (SM_{2S}, VOD_{2S}) retrievals achieved with SMOS-IC_{2S} were comparable to (SM_{TO}, VOD_{TO}) retrievals achieved with the "traditional" algorithm SMOS-IC_{TO}, all input datasets and default parameters were consistent with the original SMOS-IC_{TO} (V105) (Fernandez-Moran et al., 2017a).

2.2.2 Metrics used for evaluating SMOS-IC_{EM} retrievals

Retrievals of (*SM, VOD*) from both SMOS-IC_{TO} and SMOS-IC_{2S} were evaluated against reference datasets, and then, the resulting statistical parameters were inter-compared. Specifically, retrieved *SM* values were compared to simulated SM (SM_{ECMWF}) and *in-situ* SM measurements ($SM_{in\text{-}situ}$) and retrieved *VOD* values were compared to NDVI and AGB. For consistency and significance purposes, the following criteria were applied. Comparisons were performed: i) over a long period (i.e., 2011 – 2017) and using SMOS observations acquired during the ascending orbits (very similar results would be obtained for descending orbits (Al-Yaari et al., 2014b)); ii) strictly using the same number of pixels and the same number of data (and thus of dates) over

each pixel for the SMOS-IC$_{TO}$ and SMOS-IC$_{2S}$ retrievals; iii) applying same data filtering for the SMOS-IC$_{TO}$ and SMOS-IC$_{2S}$ retrievals, i.e., all retrievals values were filtered out for:

-SM data outside the range 0–0.6 m^3/m^3 (Dorigo et al., 2013);

-VOD data outside the range 0 – 2 (Fernandez-Moran et al., 2017a);

-Root Mean Square Error (RMSE) between $T_{\mathrm{B,mes}}^{p,\theta_j}$ and $T_{\mathrm{B},EM}^{p,\theta_j}$ exceeding 8 K, to filter out retrievals most impacted by RFI (Radio Frequency Interferences) (Al-Yaari et al., 2019b; Wigneron et al., 2018).

The evaluation of retrieved *VOD* was based on the spatial and temporal Pearson correlation coefficient (R) with ancillary vegetation indices. The evaluation of retrieved *SM* was based on four metrics which are widely used in the soil moisture community (e.g., Al-Yaari et al., 2019b; Fan et al., 2019a). These metrics include R, Root Mean Square Difference (RMSD; m^3/m^3), Bias (m^3/m^3), and the unbiased RMSD (*ub*RMSD; m^3/m^3) (Al-Yaari et al., 2019b; Entekhabi et al., 2010). It should be noted that R and *ub*RMSD were considered as primary quality criteria in comparison to Bias and RMSD, as SM_{ECMWF} and $SM_{\text{in-situ}}$ do not represent the soil moisture value as "observed" by the SMOS measurements, considering the different "sampling" depths of the simulated, retrieved and *in-situ* SM data. The mentioned metrics were computed as described in (Al-Yaari et al., 2019b). It should be noted that when comparing retrieved *SM* with $SM_{\text{in-situ}}$, the time series of satellite-based retrievals of *SM* were extracted from the original grid (i.e., 25 km) covering each site (based on latitude and longitude of the site) to obtain values corresponding to the field measurements and only the $SM_{\text{in-situ}}$ data matching with the instantaneous overpass of the SMOS observations within a time window of 1 hour were selected.

The metrics between the SMOS based retrievals of (*SM*, *VOD*) and the reference data were computed separately for each pixel/station. Each pixel/station with low quality data was

discarded from the analyses. Each pixel/station, for instance, with a number of data pairs (after filtering or quality control, e.g., only *in-situ* SM flagged as "Good" were considered) lower than one month (~31) were filtered out (Al-Yaari et al., 2019b; Kolassa et al., 2018) and only significant correlations (p-values < 0.05) were considered. As done by Al-Yaari et al. (2019b), we accounted only for *SM* retrievals where (p-value < 0.05) and (R > 0.4) when comparing to *in situ* data sets (this condition only applies to the local scale evaluation of retrieved *SM*). Finally, the median of four metrics for all pixels/stations pertaining to an IGBP land cover type or a LAI category was calculated. As correlation coefficients (R) cannot be simply averaged, we computed the median of R. In our analysis, in addition to the median skill metrics, we considered the spatial standard deviation.

3. Results

Several assessments undertaken to evaluate possible differences between *SM* and *VOD* retrievals obtained from the SMOS-IC_{TO} and SMOS-IC_{2S} algorithms are presented in this section. To this end, we inter-compared the ability of retrieved *SM* to capture the temporal dynamics of the reference SM (i.e., either SM_{ECMWF} or $SM_{in\text{-}situ}$) at both global and local scales. As there is no consensus on the reference VOD values to use at large scale (Fan et al., 2018; Fernandez-Moran et al., 2017a), retrieved *VOD* was compared to NDVI and AGB.

3.1. Retrieval evaluation at global scale

3.1.1 Soil Moisture

Global maps of the statistical parameters (i.e., R, *ub*RMSD, Bias, and RMSD) of the direct comparison of SM_{ECMWF} with SM_{2S} or with SM_{TO} over 2011 – 2017 are shown in Fig.3. Overall, when comparing to ECWMF model outputs, the spatial patterns of SM_{2S} and SM_{TO} retrievals are

very similar. According to correlation (R) results, both SM_{2S} and SM_{TO} have the same ability to capture the seasonal variations of SM_{ECMWF}. Both showed lowest R values over forested areas and both SM_{2S} and SM_{TO} yielded negative correlations with SM_{ECMWF} over some specific forest regions such as the Congo and Amazon basins and Northern Russia. The median correlations computed at global scale between the retrieved products (SM_{TO} or SM_{2S}) and SM_{ECMWF} were very similar (R = 0.63).

Similarly, no substantial difference was found in the spatial patterns of RMSD and *ub*RMSD for SM_{2S} and SM_{TO}. Specifically, over the boreal forests in Eurasia (for RMSD) and the inter-tropical regions of Africa and America (for *ub*RMSD), both SM_{2S} and SM_{TO} exhibited lower values. Similarly, for both retrieved *SM* products, there were no significant differences in the spatial patterns of Bias. Both SM_{2S} and SM_{TO} were found to be generally much drier than SM_{ECMWF}, except for northern Europe, northern Canada and some semi-arid areas (Sahara in northern Africa, and desert areas in central Asia and Australia). The general negative bias can partly result from the discrepancies between the sampling depths of the SMOS SM data (~0-3 cm top soil layer) and the top soil layer of the modelled ECMWF SM data (0-7 cm top soil layer) (Fernandez-Moran et al., 2017a). So, the different soil moisture Bias patterns shown in Fig.3 should be interpreted with caution.

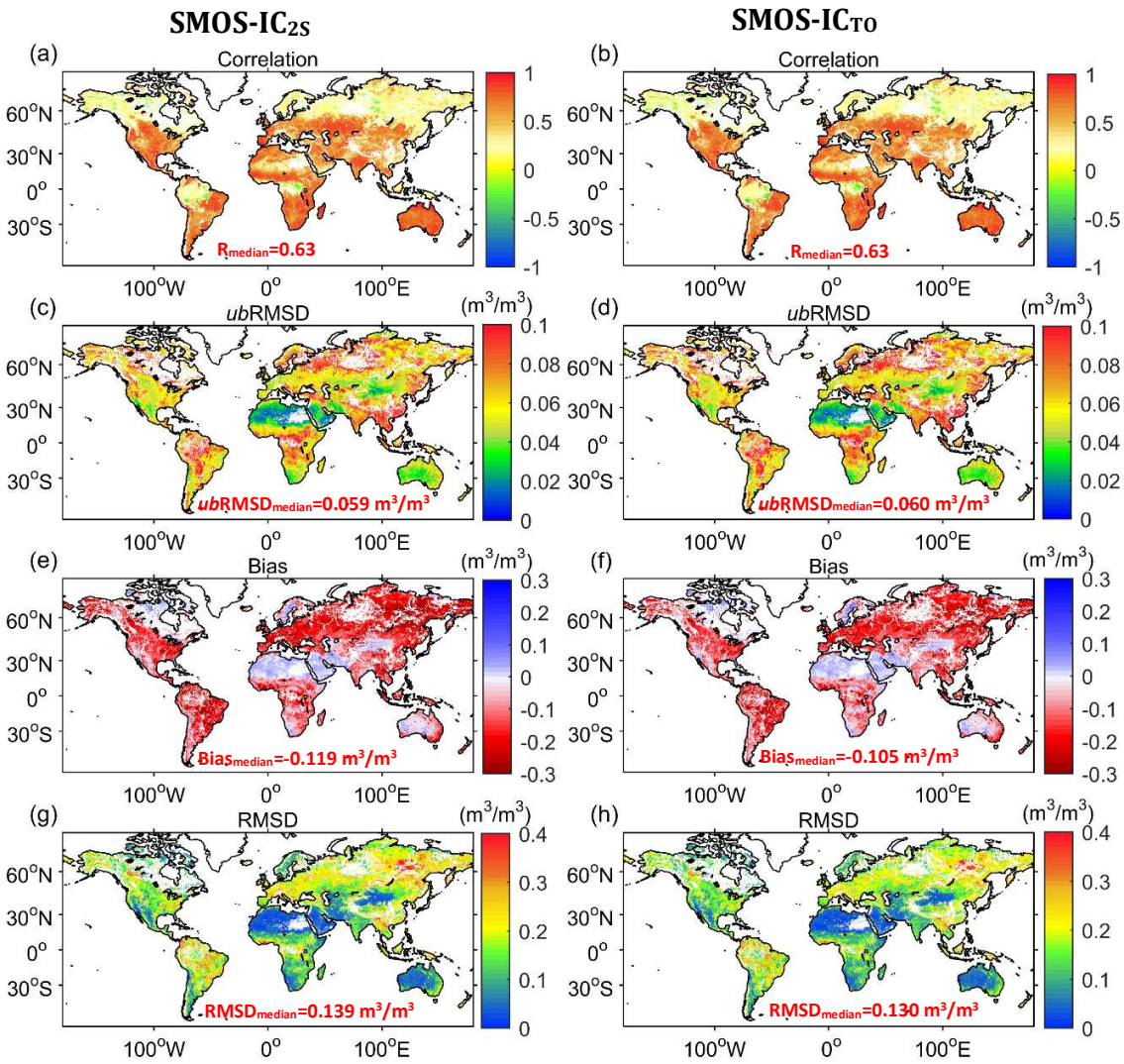

Fig. 3. Statistics at pixel-scale during 2011 – 2017 calculated between SM_{ECMWF} and SM_{TO} (Right); and SM_{2S} (Left): (a, b) correlation coefficient (R); (c, d) unbiased Root Mean Square Difference (*ub*RMSD, m^3/m^3); (e, f) Bias (m^3/m^3); (g, h) Root Mean Square Difference (RMSD, m^3/m^3).

The spatial differences between SM_{2S} and SM_{TO} in terms of Bias and *ub*RMSD are shown in Fig. S1 in the supplementary materials. It can be seen that SM_{2S} is generally drier than SM_{TO} except over the Congo Basin, Sahara in northern Africa, and desert areas in central Asia and Australia. However, *ub*RMSD for SM_{2S} is smaller than that for SM_{TO} in most of the world (except

330 in semi-arid regions of Namibia and Botswana in southern Africa and over humid areas in the
331 Amazon basin). As mentioned in Section 2.2.2, correlation and *ub*RMSD were considered as
332 primary quality criteria in this study. Thus, Fig.4 is focused on the spatial distribution of pixels
333 with the highest correlation coefficients (R) and lowest *ub*RMSD values obtained when
334 comparing SM_{ECMWF} either with $SM_{2\mathrm{S}}$ (red) or SM_{TO} (blue) over 2011 – 2017. The pixels for
335 which $|SM_{2\mathrm{S}} - SM_{\mathrm{TO}}|$ is lower than 0.02 in terms of correlation and less than 0.005 m^3/m^3 in
336 terms of *ub*RMSD are indicated by a pink color (Fernandez-Moran et al., 2017a). We found that
337 the red color is mainly distributed in the high latitudes of the northern regions, meaning that $SM_{2\mathrm{S}}$
338 is generally closer to SM_{ECMWF} in regard to the time dynamics. In some regions of the tropics
339 (mostly in the Amazon Basin and tropical Asia), SM_{TO} is performing better (blue areas) in terms
340 of R values. However, in these areas, the difference in the values of *ub*RMSD was generally
341 extremely small (<0.005 m^3/m^3, indicated by the pink color). The global maps of the temporal
342 mean SM values for the three SM datasets are shown in Fig. S2 (in the supplementary materials).
343 The spatial patterns of SM retrieved using Tau-Omega and 2S have a high similarity and both of
344 them are in good agreement with those of SM_{ECMWF} (Fig. S2a and Fig. S2b).

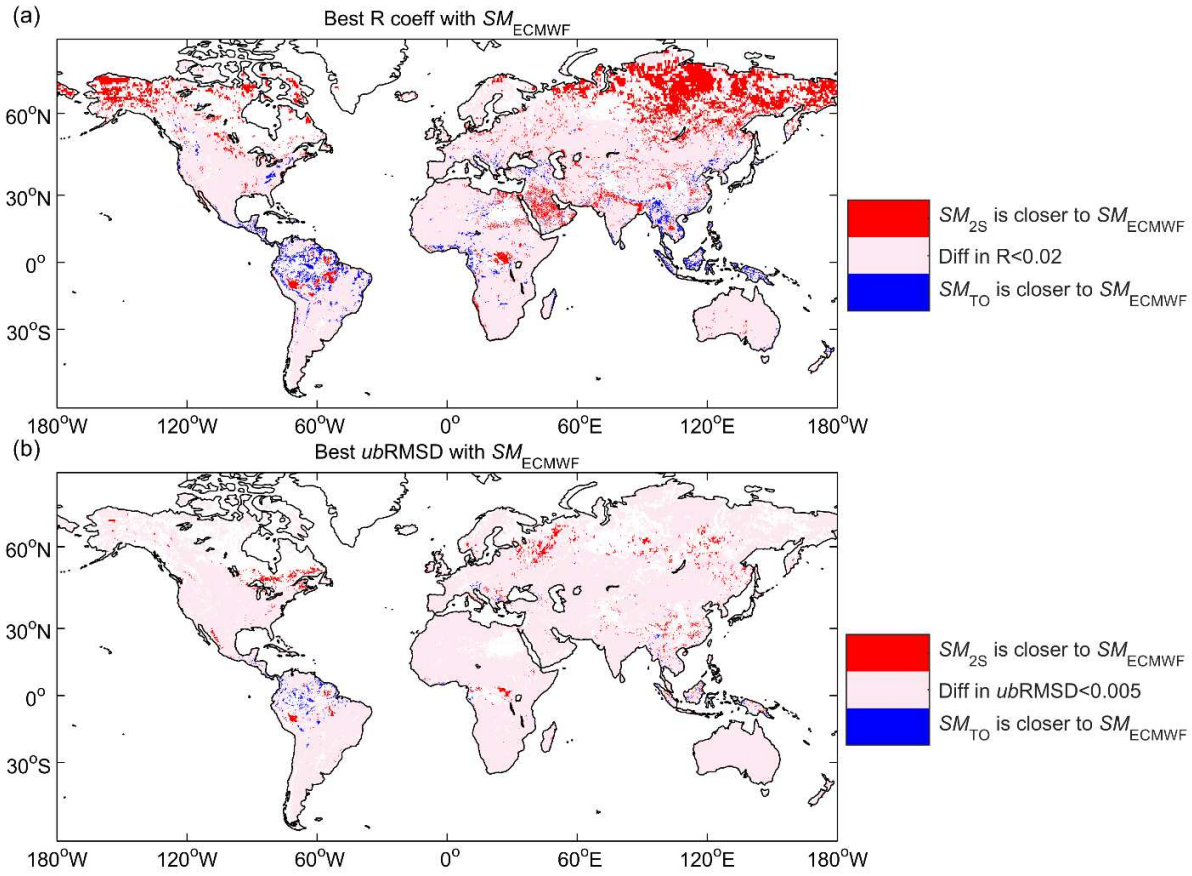

345

346 **Fig. 4.** Comparison of SM_{2S} and SM_{TO} with respect to SM_{ECMWF} showing: (a) where SM_{TO} (blue)
347 or SM_{2S} (red) provides the best correlation coefficient (R) or where the difference in R < 0.02
348 (pink); and (b) where SM_{TO} (blue) or SM_{2S} (red) leads to the lowest value of *ub*RMSD or their
349 difference in terms of *ub*RMSD < 0.005 m^3/m^3 (pink). Only pixels with significant correlation (p
350 <0.05) are presented and temporal series of data pairs >30.

351 *3.1.2 Assessment based on different vegetation conditions*

352 This section aims to evaluate and inter-compare the SM_{TO} and SM_{2S} retrievals for different
353 vegetation conditions. Fig. 5 presents the median of the statistics (i.e., R and *ub*RMSD) computed
354 between both retrieved *SM* products and SM_{ECMWF}, for MODIS-based LAI values ranging from 0
355 to 7 m^2/m^2 with an interval of 1 m^2/m^2. It can be noted that there is a decrease in correlation (R)
356 and increase in *ub*RMSD for both SM_{2S} and SM_{TO} with increasing vegetation density. Overall,
357 there was little difference between the metrics computed for SM_{2S} and SM_{TO} for the different LAI

classes. In terms of correlation (R), similar performances were obtained for SM_{2S} and SM_{TO} for the categories 0-1, 1-2 and 2-3, but a slightly better performance was obtained with SM_{TO} for LAI classes going from 3-4 to 5-7. In terms of *ub*RMSD, SM_{2S} was slightly more performant than SM_{TO} for all LAI categories.

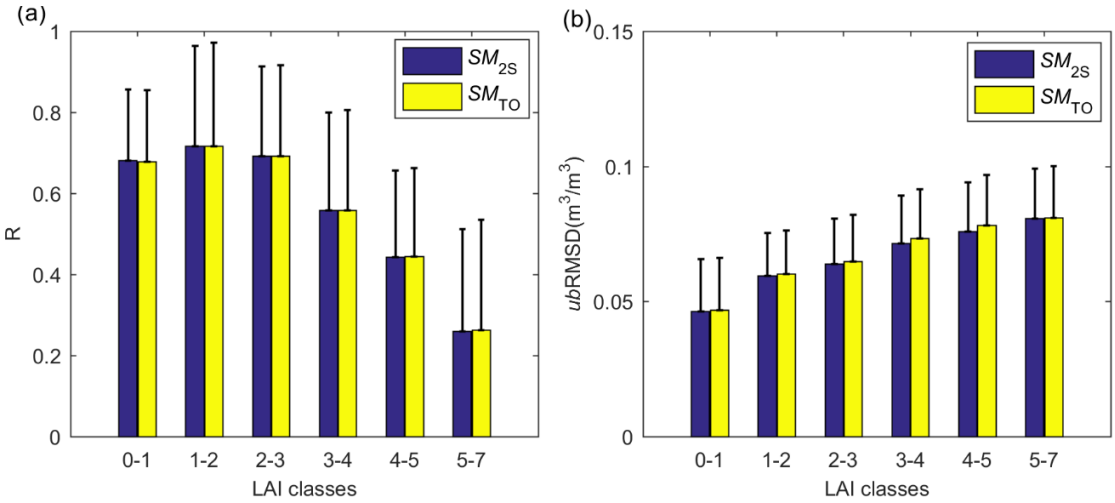

Fig. 5. Median metrics (R and *ub*RMSD, m^3/m^3) of all pixels stratified by LAI for SM_{2S} and SM_{TO} compared to SM_{ECMWF}. Error bars are represented by the standard deviation (SD) (median+SD) over each station.

Fig.6 shows the same median metrics (R and *ub*RMSD) for SM_{2S} and SM_{TO}, for all pixels stratified with the IGBP land cover type. According to correlation, it can be noted that the R values obtained with both retrieved *SM* products over non forest categories (except for "Deciduous broadleaf forests") are higher than the correlation (R) values over most of forest categories ("Evergreen broadleaf forests", "Evergreen needleleaf forests", "Deciduous needleleaf forests", and "Mixed forests"). The performance of SM_{2S} and SM_{TO} is very similar, except over "Deciduous needleleaf forests" where SM_{2S} is slightly more performant than SM_{TO}. In terms of *ub*RMSD, both SM_{2S} and SM_{TO} have relatively low values over the "Barren or sparsely vegetated" and "Shrublands" categories compared to the other land surface types. Except for "Evergreen broadleaf forests" and "Savannas" (for which results are almost similar), the *ub*RMSD obtained with SM_{2S} is lower than that obtained for SM_{TO} for all land cover types, with results over the land

types “Evergreen needleleaf forests”, “Deciduous needleleaf forests”, “Deciduous broadleaf forests”, “Mixed forests” and “Woody savannas” being the most obvious.

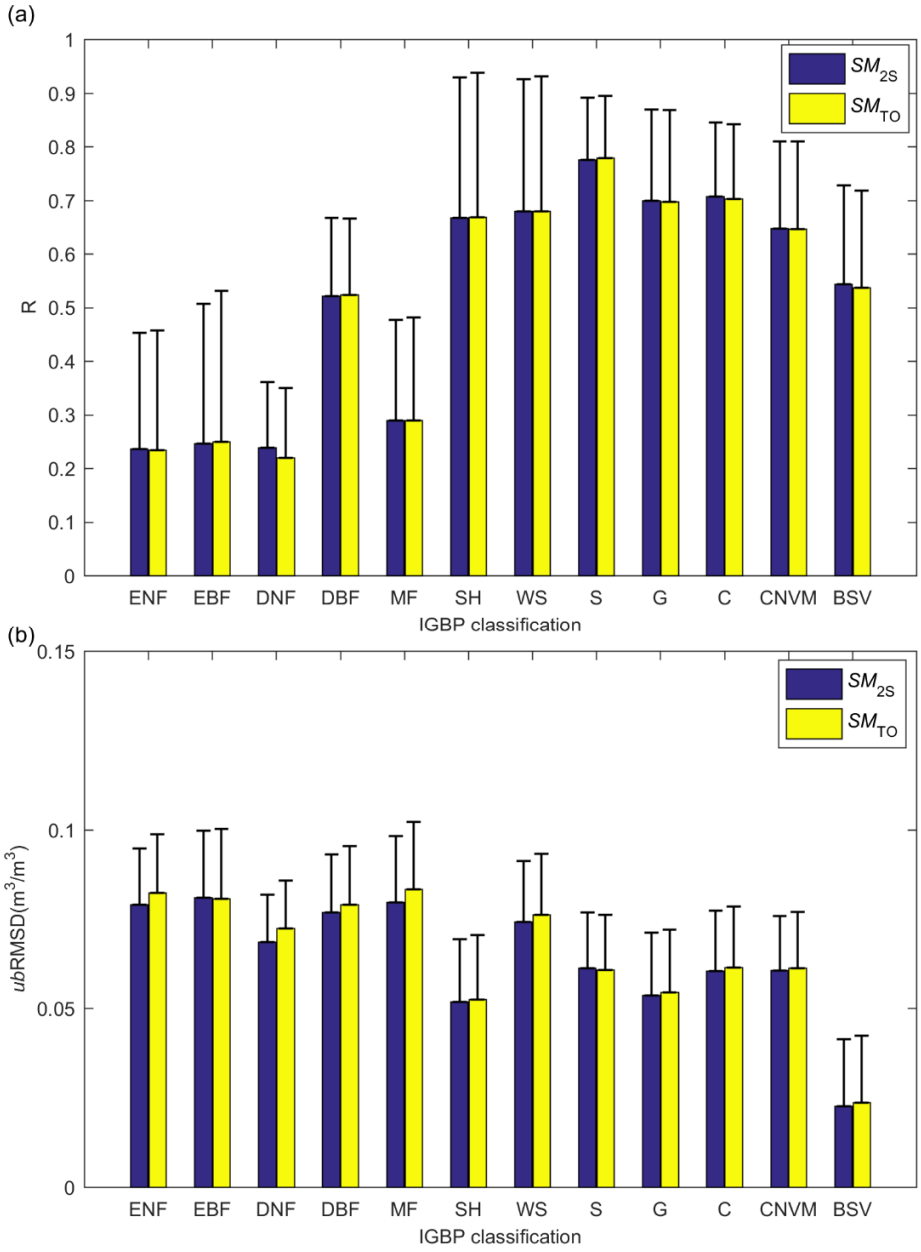

Fig. 6. Median metrics (R and *ub*RMSD, m^3/m^3) of all pixels stratified by IGBP land cover type for SM_{2S} and SM_{TO} compared to SM_{ECMWF}. With, ENF (Evergreen needleleaf forests), EBF (Evergreen broadleaf forests), DNF (Deciduous needleleaf forests), DBF (Deciduous broadleaf forests), MF (Mixed forests), SH (Shrublands), WS (Woody savannas), S (Savannas), G (Grasslands), C (Croplands), CNVM (Cropland/natural vegetation mosaics), BSV (Barren or sparsely vegetated).

3.1.3 Vegetation Optical Depth

We found that, generally, the temporal mean of VOD_{2S} and VOD_{TO} retrievals have similar spatial distribution patterns (Fig. S3). For both *VOD* retrievals, the highest VOD values were found over the tropical (e.g., over the Congo and Amazon basins) and boreal forests, and the minimum VOD values over dry areas, such as midwestern America, Sahara in northern Africa, and the desertic areas in central Asia and Australia (Fig. S3). It can be noted that the VOD_{TO} values are generally higher than those of VOD_{2S}, especially over areas covered by dense vegetation.

Fig. 7 shows the pixel-based statistics (R and Bias) derived from the direct comparison between the two VOD_{TO} and VOD_{2S} retrieved products for 2011 – 2017. In terms of correlation, VOD_{TO} and VOD_{2S} have similar ($R > 0.95$) seasonal variations at the global scale, except over tropical forests. In Fig. 7b, it can be noted that the largest differences between VOD_{TO} and VOD_{2S} are found in regions covered by dense vegetation (e.g., Amazon & Congo basins, etc.), where VOD_{2S} is found to be smaller. In these regions, the *ub*RMSD between VOD_{TO} and VOD_{2S} is also higher, contrary to barren or desert regions as in the central Asia and Australia, or in Sahara, where the *ub*RMSD values are close to zero as shown in Fig. S4.

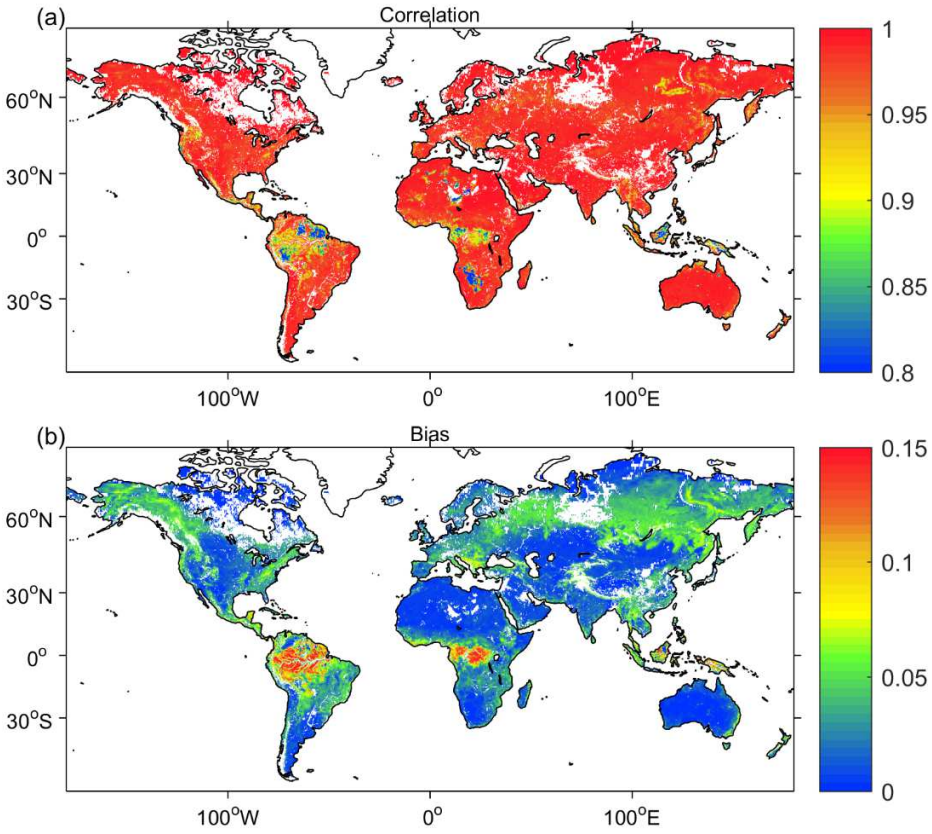

402

403 **Fig. 7.** Statistics at pixel scale during 2011 – 2017 computed between VOD_{TO} and VOD_{2S} (a)
404 correlation coefficient; (b) Bias (VOD_{TO} minus VOD_{2S}).

405 Global maps of the correlation (R) for the relationship between MODIS NDVI and 16-day
406 average values of VOD_{2S} and VOD_{TO} over 2011 – 2017 are shown in Fig.8. Overall, when
407 comparing to NDVI, the spatial patterns of VOD_{2S} and VOD_{TO} retrievals are very similar. Both
408 VOD_{2S} and VOD_{TO} showed highest R values over western Canada, Mexico, Sahel, southern
409 Africa, eastern Russia and Australia, while the lowest ones were generally found over western
410 America, eastern Europe and the border between Kazakhstan and Russia. Over most tropical
411 areas (e.g., Amazon and Congo basins), the R values between both retrieved products (VOD_{TO} or
412 VOD_{2S}) and NDVI were found to be not significant ($p > 0.05$). Moreover, as shown in Fig.3a,
413 both SM_{2S} and SM_{TO} yielded negative correlations with SM_{ECMWF} over densely-forested regions
414 in the Amazon and Congo basins. To better understand this result, we selected two sites ((15.18°

S, 62.12° W, Amazon site) in the Amazon basin and (2.45° N, 27.10° E, Congo site) in the Congo basin) corresponding to these areas to analyze and inter-compare the temporal series of NDVI and the 16-day average values of SM and VOD (Fig.S5, Table S2). SM (from all products), as shown in Fig.S5, exhibited a clear seasonal cycle, and retrieved SM (from both TO and 2S products) and ECMWF SM showed opposite interannual variations over both sites. As for SM, a clear seasonal cycle in VOD_{TO} can be noted over the Amazon site, but the seasonal cycle of VOD is generally less clear, especially at the Congo site, while NDVI showed no clear seasonal variations over both the Congo and Amazon sites. The retrieved values of VOD_{2S} and VOD_{TO} are different over both sites and both in terms of magnitude and seasonal variations, especially at the Amazon site, which is consistent with the results obtained in Fig.7. The correlation values between SM (from all products) and NDVI and that between VOD (from both TO and 2S products) and NDVI have a very low level of significance ($p > 0.1$). It is likely that this can be explained by the saturation of the NDVI values over dense vegetation, as can be clearly noted in Fig. S6. We also noted that the R values between VOD and SM (for both TO and 2S products) are generally positive and significant. This could be explained by the fact the temporal dynamics of vegetation as parameterized by VOD correspond well to the temporal dynamics of precipitation events and of the associated changes in the soil moisture values.

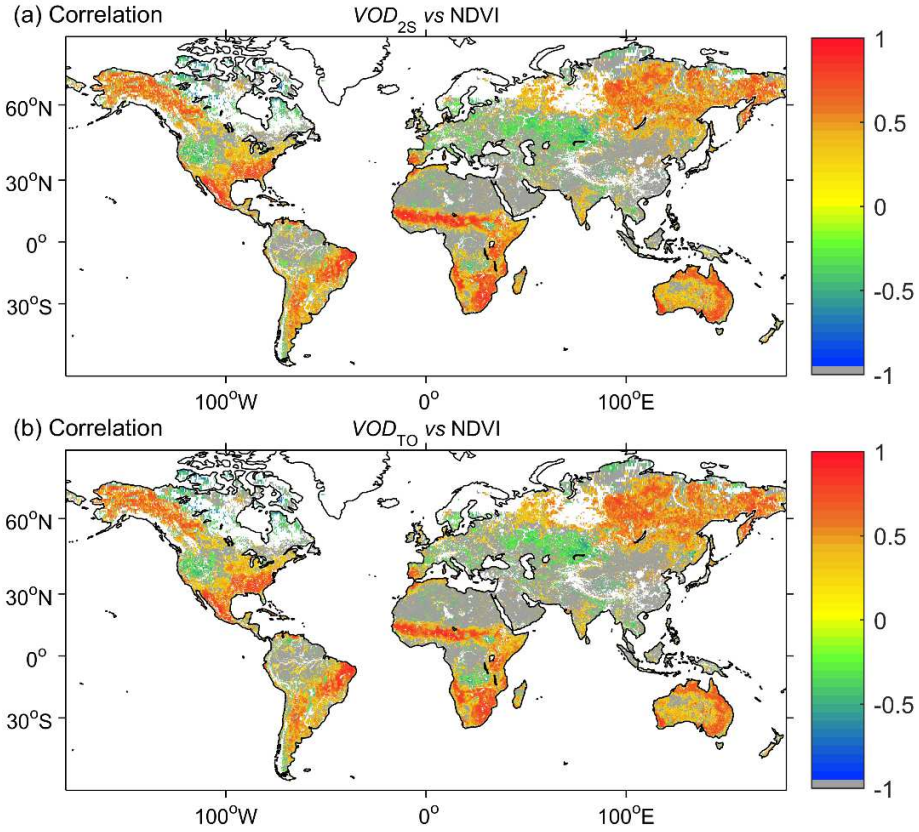

Fig. 8. Pixel-based correlation (R) for the relationship between 16-day average values of *VOD* and MODIS NDVI: (a) VOD_{2S} and (b) VOD_{TO}. Grey areas correspond to pixels where correlation is not significant as defined by a p-value > 0.05. White areas indicate "no valid data".

Fig.9 shows the spatial distribution of pixels where VOD_{2S} (red) or VOD_{TO} (blue) correlates better to MODIS NDVI during 2011-2017, (as done in Fig. 4 for SM values). Generally, the temporal correlation (R) values of VOD_{2S} were higher than those of VOD_{TO} over most of the tropical area (e.g., southern of Mexico, the marginal region of the Congo Basin), southern Australia and the northern parts of Russia and southern Europe. Conversely, in some other areas (for instance in eastern America and central Russia), a higher R value was associated with VOD_{TO}.

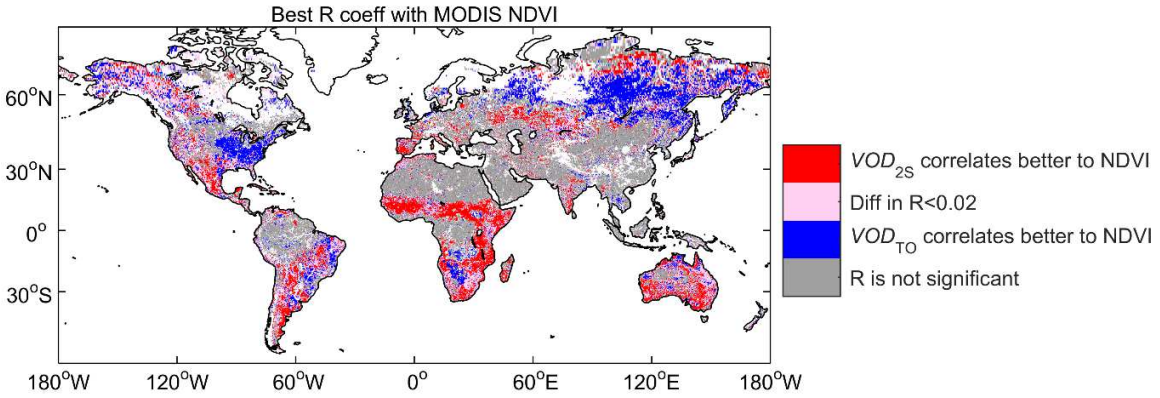

Fig. 9. Same as Fig. 4a, except that we show here the difference in correlation between 16-day average values of VOD_{2S} and VOD_{TO} with MODIS NDVI. Grey areas correspond to pixels where correlation is not significant as defined by a p-value > 0.05. White areas indicate "no valid data".

The density scatter plots between the temporal mean of retrieved *VOD* and AGB from Saatchi et al. (2011) are shown in Fig. 10. Generally, the spatial correlation obtained between the two retrieved *VOD* and AGB are very similar (R = 0.87 for both VOD_{2S} and VOD_{TO}). However, the density of higher VOD values (>1) retrieved from SMOS-IC_{2S} is lower than that retrieved from SMOS-IC_{TO} at global scale. In addition, the spatial R values computed at global scale between VOD_{2S} or VOD_{TO} with NDVI are also very similar (R = 0.66 for both VOD_{2S} and VOD_{TO}) (Fig. S6). Similarly to what was done by Rodríguez-Fernández et al. (2018) and Liu et al. (2015), we calibrated a relationship between VOD and NDVI (Fig. S6). Even though VOD and NDVI are sensitive to different features of the vegetation structure, it is interesting to note that the relationship between VOD_{2S} and NDVI has a slightly higher correlation value (difference in R ~ 0.02) than that between VOD_{TO} and NDVI. We also found that NDVI saturates even for moderate VOD values (VOD ~ 0.5), consistently with previous studies (Rodríguez-Fernández et al., 2018; Lawrence et al., 2014)(Fig. S6).

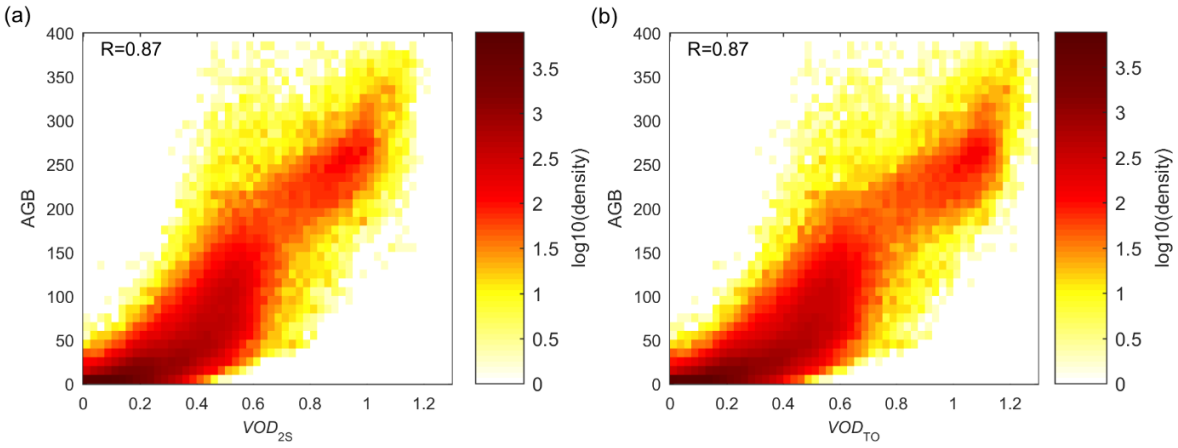

Fig. 10. Density scatter plots showing the relationship between temporal mean of retrieved VOD_{2S} (a) and VOD_{TO} (b) with above-ground biomass AGB values computed from Saatchi et al. (2011) at global scale.

3.2. Evaluation of soil moisture at local scale

To complete the global evaluation of retrieved *SM* done in Section 3.1, the performance of SM_{2S} and SM_{TO} was evaluated against $SM_{in\text{-}situ}$ at 748 *in-situ* sites over 2011 – 2017, namely the same period as that used for the global evaluation of the previous section.

Statistical results of the comparison between $SM_{in\text{-}situ}$ and both SM_{2S} and SM_{TO} are presented in Table 3. In the latter table, the median values of all metrics are given for each measurement network. From the table, we can see that the highest correlation values (R) for both SM_{2S} and SM_{TO} were obtained for FLUXNET-AMERIFLUX, while the lowest ones were found over the FMI network. For the other sites (except SWEX-POLAND, ORACLE, FR-Aqui, and UDC-SMOS), both SM_{2S} and SM_{TO} present similar results in terms of correlations. In good agreement with results of the previous sections, in terms of *ub*RMSD, same or lower values of *ub*RMSD were generally obtained with SM_{2S} (except for a few sites as SNOTEL, SWEX-POLAND, iRON). However, the difference in *ub*RMSD between SM_{2S} and SM_{TO} was generally low, and the maximum difference (0.005 m^3/m^3) was found for the MySMNet network.

In terms of median values computed over all sites ("All" item in last lines of Table 3), the metrics obtained between both products were almost the same (median *ub*RMSD of 0.061 m^3/m^3 for SM_{2S} and 0.062 m^3/m^3 for SM_{TO}; median correlation of 0.67 for both SM_{2S} and SM_{TO}). SM_{2S} and SM_{TO} had biases (remotely sensed retrievals minus *in-situ* data) with the same sign (either positive or negative) over all networks except over the MySMNet sites, where SM_{2S} was slightly drier than $SM_{in\text{-}situ}$, while SM_{TO} was much wetter than $SM_{in\text{-}situ}$. Generally, SM_{2S} was drier than SM_{TO} (median Bias of -0.061 m^3/m^3 for SM_{2S} and -0.048 m^3/m^3 for SM_{TO}).

Table 3 Statistical comparison between SM_{2S} and SM_{TO} against $SM_{in\text{-}situ}$ for 2011 – 2017. All the correlation coefficients are significant considering the criteria $p < 0.05$.

Network	*EM*	R	*ub*RMSD (m^3/m^3)	Bias (m^3/m^3)	RMSD (m^3/m^3)	Network	*EM*	R	*ub*RMSD (m^3/m^3)	Bias (m^3/m^3)	RMSD (m^3/m^3)
AMMA-CATCH	2S	0.81	0.042	0.008	0.043	CTP-SMTMN	2S	0.50	0.096	-0.049	0.108
	TO	0.82	0.042	0.007	0.043		TO	0.49	0.097	-0.041	0.105
ARM	2S	0.76	0.057	-0.137	0.150	DAHRA	2S	0.81	0.019	-0.020	0.028
	TO	0.76	0.057	-0.128	0.142		TO	0.83	0.019	-0.021	0.029
FMI	2S	0.43	0.062	0.082	0.112	SWEX-POLAND	2S	0.71	0.094	-0.237	0.255
	TO	0.43	0.065	0.111	0.134		TO	0.74	0.090	-0.220	0.238
HOBE	2S	0.66	0.053	-0.072	0.087	TERENO	2S	0.66	0.055	-0.208	0.215
	TO	0.65	0.056	-0.055	0.076		TO	0.64	0.057	-0.189	0.197
OZNET	2S	0.81	0.053	0.014	0.068	FLUXNET-AMERIFLUX	2S	0.89	0.051	-0.043	0.070
	TO	0.81	0.054	0.026	0.072		TO	0.90	0.052	-0.027	0.065
PBO-H2O	2S	0.71	0.052	-0.066	0.082	HYDROL-NET-PERUGIA	2S	0.61	0.080	-0.114	0.139
	TO	0.71	0.052	-0.057	0.078		TO	0.61	0.083	-0.089	0.121
REMEDHUS	2S	0.67	0.054	-0.035	0.075	ORACLE	2S	0.68	0.069	0.116	0.135
	TO	0.67	0.056	-0.033	0.075		TO	0.65	0.073	0.128	0.147
RISMA	2S	0.68	0.062	-0.074	0.098	VAS	2S	0.82	0.047	-0.063	0.080
	TO	0.68	0.063	-0.060	0.087		TO	0.82	0.050	-0.049	0.073
RSMN	2S	0.62	0.068	0.001	0.075	FR-Aqui	2S	0.60	0.054	-0.072	0.086
	TO	0.62	0.070	0.018	0.080		TO	0.58	0.058	-0.055	0.075
SCAN	2S	0.68	0.060	-0.054	0.096	iRON	2S	0.52	0.066	-0.198	0.219
	TO	0.68	0.061	-0.041	0.086		TO	0.53	0.065	-0.178	0.200
SMOSMANIA	2S	0.72	0.054	-0.123	0.135	BIEBRZA-S-1	2S	0.50	0.074	-0.297	0.306
	TO	0.71	0.056	-0.104	0.119		TO	0.50	0.074	-0.279	0.289
SNOTEL	2S	0.56	0.079	-0.084	0.123	MySMNet	2S	0.49	0.072	-0.003	0.072
	TO	0.56	0.078	-0.070	0.115		TO	0.48	0.077	0.022	0.082
SOILSCAPE	2S	0.79	0.057	-0.033	0.075	UDC-SMOS	2S	0.58	0.055	-0.209	0.213
	TO	0.80	0.058	-0.019	0.076		TO	0.60	0.055	-0.190	0.195
USCRN	2S	0.71	0.055	-0.063	0.100	All	2S	0.67	0.061	-0.061	0.097

	TO	0.70	0.056	-0.051	0.096		TO	0.67	0.062	-0.048	0.092

As in Section 3.1.2, in this section we also evaluated the performance (mainly based on R and *ub*RMSD) of SM_{2S} and SM_{TO} based either on LAI values ranging from 0 to 7 m^2/m^2 or IGBP land cover types and the results are reported in Fig. 11 & 12. Fig.11 shows the median value of R and *ub*RMSD computed between both retrieved *SM* products and $SM_{in\text{-}situ}$, stratified based on MODIS LAI categories. It can be seen that, as already observed in Fig. 5, there is a decrease in correlation (R) and increase in *ub*RMSD for both SM_{2S} and SM_{TO} with increasing vegetation density when compared to $SM_{in\text{-}situ}$. In terms of R, SM_{2S} performs better than SM_{TO} in category 2-3, and vice versa in category 5-7. SM_{2S} and SM_{TO} have a similar performance over the categories 0-1, 1-2, 3-4 and 4-5. When focusing on *ub*RMSD (Fig. 11b), SM_{2S} performs slightly better or similarly as SM_{TO} over the LAI categories ranging from 0-1 to 5-7. However, unlike the results presented in Fig. 5, the difference between SM_{2S} and SM_{TO} is most pronounced for category 5-7.

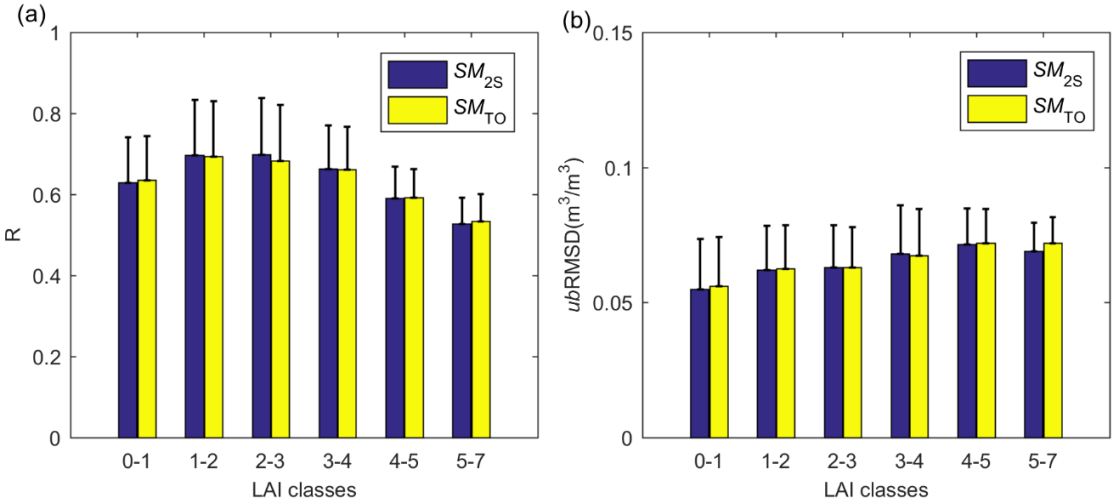

Fig. 11. Median metrics (R and *ub*RMSD, m^3/m^3) of all sites stratified by LAI for SM_{2S} and SM_{TO} compared to $SM_{in\text{-}situ}$. Number of stations (n) per category: 0-1 (n = 203 stations), 1-2 (n = 282 stations), 2-3 (n = 173 stations), 3-4 (n = 58 stations), 4-5 (n = 26 stations), 5-7 (n = 6 stations).

Another insight on the effect of vegetation on the accuracy of the retrieved *SM* products with respect to $SM_{in\text{-}situ}$ are shown in Fig. 12. In terms of R, both SM_{2S} and SM_{TO} have the lowest

506 variability in their performances amongst all stations, as evaluated by standard deviation, over the
507 “Barren or sparsely vegetated” categories. As already observed in Fig. 6, the performance of
508 SM_{2S} and SM_{TO} is almost the same, except over “Croplands”, “Barren or sparsely vegetated” and
509 “Grasslands”. More generally, it can be noted that the R values obtained with SM_{2S} are higher or
510 similar to those of SM_{TO} for all land cover categories (except “Grasslands”), with best results
511 over the land covers “Evergreen broadleaf forests”, “Croplands” and "Barren or sparsely
512 vegetated". In terms of *ub*RMSD, both SM_{2S} and SM_{TO} have relatively small values over the
513 “Barren or sparsely vegetated” and “Shrublands” categories compared to the other land surface
514 types, and this is also consistent with the results of Fig. 6. It can be noted that the *ub*RMSD
515 obtained with SM_{2S} is lower or equal to that of SM_{TO} for all land cover categories, with best
516 results over the land covers “Evergreen broadleaf forests”, “Shrublands”, “Woody savannas” and
517 “Croplands”.

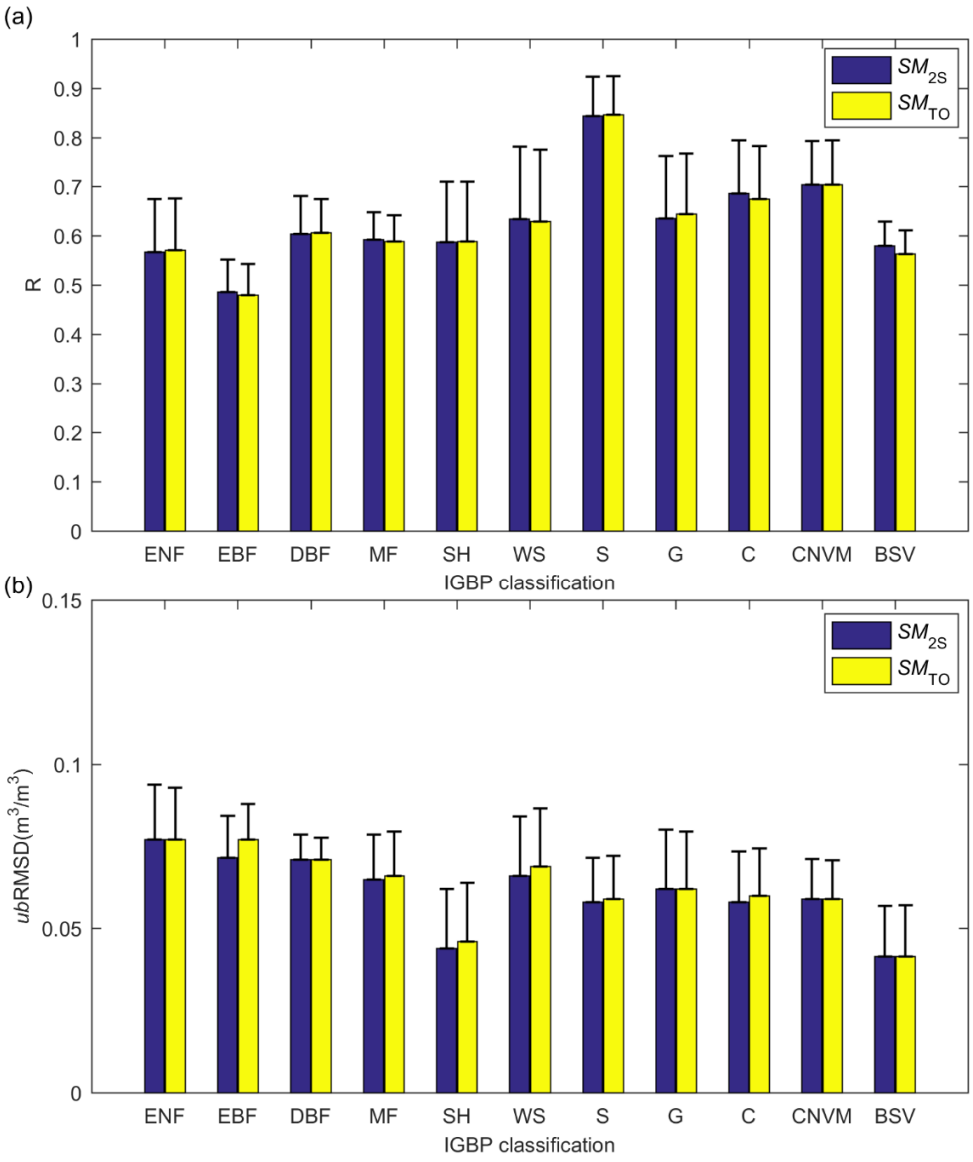

Fig.12. Same as Fig. 6, except that SM_{2S} and SM_{TO} are compared to $SM_{in\text{-}situ}$. Number of stations per category: ENF (n = 49 station), EBF (n = 4 station), DBF (n = 9 station), MF (n = 13 station), SH (n = 53 stations), WS (n = 37 stations), S (n = 84 stations), G (n = 284 stations), C (n = 152 stations), CNVM (n = 57 stations), BSV (n = 6 stations).

4. Discussion

The evaluation results of this study generally show that the performance of the two SMOS-IC$_{TO}$ and SMOS-IC$_{2S}$ retrieval algorithms are generally very similar (Figs. S2, 3, 4 & Table 3),

whether we consider the spatial patterns of the temporal mean SM values or the values of the metrics (i.e., R, *ub*RMSD, Bias and RMSD). This result was obtained from the comparison of SM_{2S} and SM_{TO} with both modelled (SM_{ECMWF}) and *in-situ* ($SM_{in\text{-}situ}$) data.

The fact that the performances of the two SMOS-IC_{TO} and SMOS-IC_{2S} algorithms were generally very similar can be considered as surprising at first sight as Tau-Omega is only a 0^{th}-order solution of the RT equations, while 2S is a 1^{st}-order solution that accounts for multiple scattering and reflection effects. However, as discussed in Wigneron et al. (2017), some studies (e.g., Kurum, 2013; Mo et al., 1982) have shown that the analytical form of the equations of the Tau-Omega model incorporates multiple-scattering effects up to first-order, provided the parameters ω and τ (VOD) are considered as effective parameters. So, as the values of ω and τ (VOD) are effective values in the SMOS-IC algorithm (as computed from best-fit approaches (Fernandez-Moran et al., 2017a; Fernandez-Moran et al., 2017b)), the Tau-Omega model equations implicitly account for multiple scattering effects up to first-order.

These considerations may allow us to explain the two main results of the study (1) the low difference in the performances between the SMOS-IC_{TO} and SMOS-IC_{2S} algorithms (2) the differences obtained in the values of retrieved VOD for both the Tau-Omega and 2S algorithms. Considering the latter point, the main differences (VOD_{2S} smaller than VOD_{TO}) could be noted, especially in dense tropical forests of the Amazon and Congo basins, and to a smaller extent, in the boreal regions.

We can explain Point (1) by the fact that the Tau-Omega model equations are valid to first-order, as discussed above. Moreover, we should not forget that radiative transfer modelling (even considering first-order or multiple-order scattering effects) is still an approximation as it corresponds to incoherent modelling, where only the intensity of the radiations is accounted for

(in contrast to coherent approaches, accounting for both the amplitude and phase of the microwave radiations, which are more precise but more complex). This latter point may also provide a partial explanation to the low difference in performance found between the Tau-Omega and 2S retrievals.

Point (2) can be explained by the fact that, as discussed above, the retrieved value of VOD using Tau-Omega is effective, and may not be directly comparable with the retrieved value using 2S. The latter value can be considered as more "accurate" and less "effective", as 2S does not make several simplifications considered Tau-Omega. It is interesting to note that the largest differences between VOD_{2S} and VOD_{TO} were obtained in dense forests (i.e. for high VOD values) where multiple scattering effects are expected to be most prominent (and where the validity of the Tau-Omega modelling is the most critical).

Contrary to SM, evaluating the accuracy of the retrieved VOD values at the global scale is difficult as there is no consensus on the reference values to use at large spatial scales from models or *in-situ* data. We used here two main vegetation parameters: MODIS NDVI and above-ground biomass (AGB) to evaluate the VOD_{2S} and VOD_{TO} retrievals. The evaluation was based on a correlation analysis, in temporal terms for NDVI and spatial terms for biomass. Over low vegetation types, it has often been considered that VOD and NDVI (and LAI) are strongly correlated in terms of seasonal dynamics (Wigneron et al., 2017 for a review). Over woody vegetation, it has often been considered that the yearly values of VOD and vegetation biomass are strongly correlated (Brandt et al., 2018; Wigneron et al., 2017 for a review). So, even though the two parameters (NDVI and biomass) we used in the present study are not "reference" data, they are relatively complementary to evaluate the *VOD* retrievals as (i) NDVI could be

572 considered as more pertinent for low vegetation canopies and (ii) yearly average biomass could
573 be considered as more pertinent for woody vegetation types.

574 5. Conclusion

575 We evaluated in this study the performances of two emission models (Tau-Omega and 2S) in
576 the SMOS-IC algorithm. We inter-compared the *SM* retrievals from SMOS-IC against the
577 ECMWF modelled SM (SM_{ECMWF}) and the ISMN ground-based measurements ($SM_{in\text{-}situ}$) for
578 different vegetation conditions at both global and local scales, while retrieved *VOD* was
579 evaluated against the NDVI and AGB vegetation features. The inter-comparison was based on
580 the correlation coefficient (R), RMSD, Bias and *ub*RMSD metrics. We present below the main
581 conclusions that can be drawn from the results:

582 (i) both SM_{2S} and SM_{TO} products are generally found to be drier than SM_{ECMWF} and $SM_{in\text{-}situ}$,
583 while SM_{2S} is found to be drier than SM_{TO} by ~ 0.015 m^3/m^3 in average at global scale.
584 However, the different sampling layers considered for SM_{ECMWF}, $SM_{in\text{-}situ}$ and for the SMOS
585 SM retrievals, makes it difficult to accurately evaluate the performance of the retrieved *SM*
586 data in terms of Bias (Fernandez-Moran et al., 2017a).

587 (ii) both SM_{2S} and SM_{TO} have a similar ability to capture the seasonal variations in SM_{ECMWF} and
588 $SM_{in\text{-}situ}$. Specifically, the median R values computed at global scale between both retrieved
589 *SM* products (SM_{2S} or SM_{TO}) with SM_{ECMWF} are very close (R = 0.63 for both retrieved *SM*
590 products); idem for the median correlation between SM_{2S} and SM_{TO} with $SM_{in\text{-}situ}$ computed
591 over all ISMN sites (R = 0.67 for both retrieved *SM* products).

(iii) the *ub*RMSD obtained with SM_{2S} is always lower or similar (for "Evergreen broadleaf forest" and "Savannas" in Fig. 6) than that obtained with SM_{TO} over all IGBP land cover types when compared to the reference SM.

(iv) retrieved VOD_{2S} and VOD_{TO} have similar ($R > 0.95$) seasonal variations at global scale except for tropical forests, and a large Bias (> 0.1) between VOD_{2S} and VOD_{TO} was found over the tropical forest (VOD_{2S} is smaller than VOD_{TO}).

(v) the temporal correlation (R) values obtained by comparing VOD_{2S} and NDVI are generally higher than those obtained by comparing VOD_{TO} and NDVI over most tropical areas, southern Australia, some northern parts of Russia and southern Europe. The spatial correlation (R) values between retrieved VOD_{2S} or VOD_{TO} and the reference datasets (NDVI: $R = 0.66$; AGB: $R = 0.87$ for both retrieved *VOD* products) are very similar.

As summarized above, retrieved products (SM or VOD) achieved with the Tau-Omega and 2S models are generally very close in terms of temporal or spatial correlations. It is one of the first times that a study show that at global scale, and as predicted by Kurum (2013), there is a low difference between retrieval results obtained from the inversion of the Tau-Omega (0^{th}-order solution of the RT equations) or 2S (1^{st}-order solution of the RT equations) models. However, and this is a key point mentioned in the introduction, as 2S is more "physical" than Tau-Omega and thus allows using a unified emission model for different applications (e.g., surface soil moisture, vegetation optical depth, soil permittivity or snow status) (Derek et al, submitted; Schwank et al., 2018; Wigneron et al., 2017), 2S appears to be a very interesting option for future versions of SMOS-IC. The results obtained here with SMOS observations should also be applicable to other microwave sensors in space, such as the NASA SMAP mission even though no tests were made here with SMAP observations. It should be noted that even though the

performances of both TO and 2S are comparable, we highlighted that the retrieved values of VOD and SM from both models are not quite similar. For instance, VOD values retrieved from the two models vary a lot over dense vegetation areas, both in terms of magnitude and seasonal variations (Fig. 7 and Fig. S5). As VOD is used more and more in key applications, for example in analyzing carbon sinks and emissions (Brandt et al., 2018; Fan et al., 2019b), and in monitoring vegetation water stress (Konings and Gentine, 2017; Tian et al., 2018) the difference in the values of VOD_{2S} and VOD_{TO} over dense vegetation may have strong implications. For instance, a difference in the value of VOD larger than 0.1 over the Amazon study (as revealed in the present study), represents several billions of tons of carbons stocks. So the difference obtained in the VOD retrievals between 2S and TO may have a huge importance when considering applications to the monitoring of the global carbon cycle. Further analyses are required to identify which product (VOD_{2S} or VOD_{TO}) is the most accurate and appropriate for a range of applications.

Appendix

SMOS-IC algorithm based on Tau-Omega and Two-Stream

The SMOS-IC_{2S} algorithm is very similar to the "traditional" SMOS-IC_{TO} algorithm (corresponding to the actual V105 versions), except that 2S is used instead of Tau-Omega to simulate brightness temperatures $T_{B,EM}^{p,\theta}$. Note that the effects of the atmosphere are neglected in this study. In the 2-Parameter retrievals of (SM_{EM}, VOD_{EM}) carried out with SMOS-IC_{EM}, the effective scattering albedo ω_{EM} is considered as constant according to different land cover types

(Table 1 in Fernandez-Moran et al. (2017a)). Both SMOS-IC$_{TO}$ and SMOS-IC$_{2S}$ retrievals of SM and VOD involve the minimization of the following Cost Function (*CF*):

$$CF(SM_{EM}, \tau_{EM}) = \frac{1}{\sigma T_B{}^2} \sum_{i=1}^{N} (T_{B,mes}^{p,\theta_j} - T_{B,EM}^{p,\theta_j})^2 + \frac{1}{\sigma P_i^2} \sum_{P=\{SM_{EM},\tau_{EM}\}} (P^{ini} - P)^2 \quad (1)$$

where N is the number of observations at different nadir angles θ_i, $T_{B,mes}^{p,\theta_j}$ and σT_B are the measured brightness temperatures obtained from the SMOS-L3 products with associated standard deviations, $T_{B,EM}^{p,\theta_j}$ are brightness temperatures simulated with EM = TO or EM = 2S. The second term in CF is a regularization function including the retrieval parameters $P = \{SM_{EM}, \tau_{EM}\}$ and their priori estimates $P^{ini} = \{SM_{EM}^{ini}, \tau_{EM}^{ini}\}$.

Acknowledgments

This work was supported by both CNES, France (Centre National d'Etudes Spatiales) and the China Scholarship Council (CSC). The physical basis needed to replace the Tau-Omega with the Two-Stream emission model in SMOS-IC was laid within research performed by the "SMOS Expert Support Laboratory (ESL) for Level-2 Soil Moisture" funded by the ESA (European Space Agency) contract No.: 4000113119/15/I-SB0. The authors would like to thank CATDS (Centre Aval de Traitement des Données SMOS) and ESA for providing SMOS TB products and the ISMN for supporting *in-situ* soil moisture. The authors would also like to thank Dr. Dara Entekhabi, Professor, from Department of Civil and Environmental Engineering, Massachusetts Institute of Technology and Dr. Alexandra G. Konings, Assistant Professor, from Department of Earth System Science, Stanford University for spending his/her valuable time for reading the manuscripts and providing valuable suggestions. Xiaojun Li was sponsored by China Scholarship

Council (CSC), and especially wish to thank his father, Yuhua Li and his mother, Fengnian Zhan, for giving him inimitable support.

References

Al-Yaari, A., Ducharne, A., Cheruy, F., Crow, W., & Wigneron, J.-P. (2019a). Satellite-based soil moisture provides missing link between summertime precipitation and surface temperature biases in CMIP5 simulations over conterminous United States. *Scientific reports, 9*, 1657.

Al-Yaari, A., Wigneron, J.-P., Dorigo, W., Colliander, A., Pellarin, T., Hahn, S., Mialon, A., Richaume, P., Fernandez-Moran, R., & Fan, L. (2019b). Assessment and inter-comparison of recently developed/reprocessed microwave satellite soil moisture products using ISMN ground-based measurements. *Remote Sensing of Environment, 224*, 289-303.

Al-Yaari, A., Wigneron, J.-P., Ducharne, A., Kerr, Y., De Rosnay, P., De Jeu, R., Govind, A., Al Bitar, A., Albergel, C., & Munoz-Sabater, J. (2014a). Global-scale evaluation of two satellite-based passive microwave soil moisture datasets (SMOS and AMSR-E) with respect to Land Data Assimilation System estimates. *Remote Sensing of Environment, 149*, 181-195.

Al-Yaari, A., Wigneron, J.-P., Ducharne, A., Kerr, Y., Wagner, W., De Lannoy, G., Reichle, R., Al Bitar, A., Dorigo, W., & Richaume, P. (2014b). Global-scale comparison of passive (SMOS) and active (ASCAT) satellite based microwave soil moisture retrievals with soil moisture simulations (MERRA-Land). *Remote Sensing of Environment, 152*, 614-626.

Al-Yaari, A., Wigneron, J.-P., Kerr, Y., Rodriguez-Fernandez, N., O'Neill, P., Jackson, T., De Lannoy, G., Al Bitar, A., Mialon, A., & Richaume, P. (2017). Evaluating soil moisture retrievals from ESA's SMOS and NASA's SMAP brightness temperature datasets. *Remote Sensing of Environment, 193*, 257-273.

Al Bitar, A., Mialon, A., Kerr, Y.H., Cabot, F., Richaume, P., Jacquette, E., Quesney, A., Mahmoodi, A., Tarot, S., & Parrens, M. (2017). The global SMOS Level 3 daily soil moisture and brightness temperature maps. *Earth System Science Data, 9*, 293-315.

Albergel, C., De Rosnay, P., Gruhier, C., Muñoz-Sabater, J., Hasenauer, S., Isaksen, L., Kerr, Y., & Wagner, W. (2012). Evaluation of remotely sensed and modelled soil moisture products using global ground-based in situ observations. *Remote Sensing of Environment, 118*, 215-226.

Albergel, C., Rüdiger, C., Pellarin, T., Calvet, J.-C., Fritz, N., Froissard, F., Suquia, D., Petitpa, A., Piguet, B., & Martin, E. (2008). From near-surface to root-zone soil moisture using an exponential filter: an assessment of the method based on in-situ observations and model simulations. *Hydrology and Earth System Sciences, 12*, 1323-1337.

Bell, J.E., Palecki, M.A., Baker, C.B., Collins, W.G., Lawrimore, J.H., Leeper, R.D., Hall, M.E., Kochendorfer, J., Meyers, T.P., & Wilson, T. (2013). US Climate Reference Network soil moisture and temperature observations. *Journal of Hydrometeorology, 14*, 977-988.

Berrisford, P., Kållberg, P., Kobayashi, S., Dee, D., Uppala, S., Simmons, A., Poli, P., & Sato, H. (2011). Atmospheric conservation properties in ERA-Interim. *Quarterly Journal of the Royal Meteorological Society, 137*, 1381-1399.

Brandt, M., Wigneron, J.-P., Chave, J., Tagesson, T., Penuelas, J., Ciais, P., Rasmussen, K., Tian, F., Mbow, C., & Al-Yaari, A. (2018). Satellite passive microwaves reveal recent climate-induced carbon losses in African drylands. *Nature ecology & evolution, 2*, 827.

Broxton, P.D., Zeng, X., Sulla-Menashe, D., & Troch, P.A. (2014). A global land cover climatology using MODIS data. *Journal of Applied Meteorology and Climatology, 53*, 1593-1605.

Calvet, J.-C., Fritz, N., Froissard, F., Suquia, D., Petitpa, A., & Piguet, B. (2007). In situ soil moisture observations for the CAL/VAL of SMOS: The SMOSMANIA network. In, *2007 IEEE International Geoscience and Remote Sensing Symposium* (pp. 1196-1199): IEEE.

Chaparro, D., Piles, M., Vall-Llossera, M., Camps, A., Konings, A.G., & Entekhabi, D. (2018). L-band vegetation optical depth seasonal metrics for crop yield assessment. *Remote Sensing of Environment, 212*, 249-259.

Colliander, A., Kerr, Y., Wigneron, J.P., Al-Yaari, A., Rodriguez-Fernandez, N., Neill, P.O., jackson, T.J., Yueh, S.H., Asanuma, J., Berg, A.A., Bosch, D.D., Caldwell, T., Cosh, M.H., Holifield Collins, C., Jensen, K.H., Martínez-Fernández, J., McNairn, H., J.H., P., Pulliainen, J., Seyfried, M., Starks, P.J., Su, Z., Thibeault, M., & Walker, J.P. (in prepration). Intercomparison of SMOS and SMAP Soil Moisture Products over Core Validation Sites In, *European Space Agency's 2019 Living Plant Symposium.*

Dee, D.P., Uppala, S., Simmons, A., Berrisford, P., Poli, P., Kobayashi, S., Andrae, U., Balmaseda, M., Balsamo, G., & Bauer, d.P. (2011). The ERA-Interim reanalysis: Configuration and performance of the data assimilation system. *Quarterly Journal of the Royal Meteorological Society, 137*, 553-597.

Derek Houtz, Reza Naderpour, Mike Schwank, Konrad Steffen, Snow Wetness and Density Retrieved from L-band Satellite Radiometer Observations over a Site in the West Greenland Ablation Zone. *Remote Sensing of Environment, submitted in April 2019*.

Derksen, C., Xu, X., Dunbar, R.S., Colliander, A., Kim, Y., Kimball, J.S., Black, T.A., Euskirchen, E., Langlois, A., & Loranty, M.M. (2017). Retrieving landscape freeze/thaw state from Soil Moisture Active Passive (SMAP) radar and radiometer measurements. *Remote Sensing of Environment, 194*, 48-62.

Dorigo, W., Gruber, A., De Jeu, R., Wagner, W., Stacke, T., Loew, A., Albergel, C., Brocca, L., Chung, D., & Parinussa, R. (2015). Evaluation of the ESA CCI soil moisture product using ground-based observations. *Remote Sensing of Environment, 162*, 380-395.

Dorigo, W., Wagner, W., Albergel, C., Albrecht, F., Balsamo, G., Brocca, L., Chung, D., Ertl, M., Forkel, M., & Gruber, A. (2017). ESA CCI Soil Moisture for improved Earth system understanding: State-of-the art and future directions. *Remote Sensing of Environment, 203*, 185-215.

Dorigo, W., Wagner, W., Hohensinn, R., Hahn, S., Paulik, C., Xaver, A., Gruber, A., Drusch, M., Mecklenburg, S., & Oevelen, P.v. (2011). The International Soil Moisture Network: a data hosting facility for global in situ soil moisture measurements. *Hydrology and Earth System Sciences, 15*, 1675-1698.

Dorigo, W., Xaver, A., Vreugdenhil, M., Gruber, A., Hegyiova, A., Sanchis-Dufau, A., Zamojski, D., Cordes, C., Wagner, W., & Drusch, M. (2013). Global automated quality control of in situ soil moisture data from the International Soil Moisture Network. *Vadose Zone Journal, 12*

Ebrahimi-Khusfi, M., Alavipanah, S.K., Hamzeh, S., Amiraslani, F., Samany, N.N., & Wigneron, J.-P. (2018). Comparison of soil moisture retrieval algorithms based on the synergy between SMAP and SMOS-IC. *International journal of applied earth observation and geoinformation, 67*, 148-160.

Entekhabi, D., Njoku, E.G., O'Neill, P.E., Kellogg, K.H., Crow, W.T., Edelstein, W.N., Entin, J.K., Goodman, S.D., Jackson, T.J., & Johnson, J. (2010). The soil moisture active passive (SMAP) mission. *Proceedings of the IEEE, 98*, 704-716.

Fan, L., Wigneron, J.-P., Xiao, Q., Al-Yaari, A., Wen, J., Martin-StPaul, N., Dupuy, J.-L., Pimont, F., Al Bitar, A., & Fernandez-Moran, R. (2018). Evaluation of microwave remote sensing for monitoring live fuel moisture content in the Mediterranean region. *Remote Sensing of Environment, 205*, 210-223.

Fan, L., Al-Yaari, A., Frappart, F., Swenson, J.J., Xiao, Q., Wen, J., Jin, R., Kang, J., Li, X., & Fernandez-Moran, R. (2019a). Mapping Soil Moisture at a High Resolution over Mountainous Regions by Integrating In Situ Measurements, Topography Data, and MODIS Land Surface Temperatures. *Remote Sensing, 11*, 656.

Fan, L., Wigneron, J.-P., Ciais, P., Chave, J., Brandt, M., Fensholt, R., Saatchi, S.S., Bastos, A., Al-Yaari, A., & Hufkens, K. (2019b). Satellite-observed pantropical carbon dynamics. *Nature plants*, 1.

Feldman, A.F., Akbar, R., & Entekhabi, D. (2018). Characterization of higher-order scattering from vegetation with SMAP measurements. *Remote Sensing of Environment, 219*, 324-338.

751 Fernandez-Moran, R., Al-Yaari, A., Mialon, A., Mahmoodi, A., Al Bitar, A., De Lannoy, G., Rodriguez-
752 Fernandez, N., Lopez-Baeza, E., Kerr, Y., & Wigneron, J.-P. (2017a). SMOS-IC: An alternative
753 SMOS soil moisture and vegetation optical depth product. *Remote Sensing, 9*, 457.
754 Fernandez-Moran, R., Wigneron, J.-P., De Lannoy, G., Lopez-Baeza, E., Parrens, M., Mialon, A.,
755 Mahmoodi, A., Al-Yaari, A., Bircher, S., & Al Bitar, A. (2017b). A new calibration of the effective
756 scattering albedo and soil roughness parameters in the SMOS SM retrieval algorithm. *International*
757 *journal of applied earth observation and geoinformation, 62*, 27-38.
758 Ferrazzoli, P., Guerriero, L., & Wigneron, J.-P. (2002). Simulating L-band emission of forests in view of
759 future satellite applications. *IEEE transactions on Geoscience and remote sensing, 40*, 2700-2708.
760 Guglielmetti, M., Schwank, M., Matzler, C., Oberdorster, C., Vanderborght, J., & Fluhler, H. (2008).
761 FOSMEX: Forest soil moisture experiments with microwave radiometry. *IEEE transactions on*
762 *Geoscience and remote sensing, 46*, 727-735.
763 Holben, B.N. (1986). Characteristics of maximum-value composite images from temporal AVHRR data.
764 *International journal of remote sensing, 7*, 1417-1434.
765 Hornbuckle, B.K., Patton, J.C., VanLoocke, A., Suyker, A.E., Roby, M.C., Walker, V.A., Iyer, E.R.,
766 Herzmann, D.E., & Endacott, E.A. (2016). SMOS optical thickness changes in response to the
767 growth and development of crops, crop management, and weather. *Remote Sensing of Environment,*
768 *180*, 320-333.
769 Jackson, T.J. (1993). III. Measuring surface soil moisture using passive microwave remote sensing.
770 *Hydrological processes, 7*, 139-152.
771 Jackson, T.J., Cosh, M.H., Bindlish, R., Starks, P.J., Bosch, D.D., Seyfried, M., Goodrich, D.C., Moran,
772 M.S., & Du, J. (2010). Validation of advanced microwave scanning radiometer soil moisture products.
773 *IEEE transactions on Geoscience and remote sensing, 48*, 4256-4272.
774 Jackson, T.J., Schmugge, T.J., & Wang, J.R. (1982). Passive microwave sensing of soil moisture under
775 vegetation canopies. *Water Resources Research, 18*, 1137-1142.
776 Jung, M., Reichstein, M., Schwalm, C.R., Huntingford, C., Sitch, S., Ahlström, A., Arneth, A., Camps-
777 Valls, G., Ciais, P., & Friedlingstein, P. (2017). Compensatory water effects link yearly global land
778 CO 2 sink changes to temperature. *Nature, 541*, 516.
779 Kerr, Y.H., Waldteufel, P., Wigneron, J.-P., Delwart, S., Cabot, F., Boutin, J., Escorihuela, M.-J., Font, J.,
780 Reul, N., & Gruhier, C. (2010). The SMOS mission: New tool for monitoring key elements ofthe
781 global water cycle. *Proceedings of the IEEE, 98*, 666-687.
782 Kerr, Y.H., Waldteufel, P., Wigneron, J.-P., Martinuzzi, J., Font, J., & Berger, M. (2001). Soil moisture
783 retrieval from space: The Soil Moisture and Ocean Salinity (SMOS) mission. *IEEE transactions on*
784 *Geoscience and remote sensing, 39*, 1729-1735.
785 Kolassa, J., Reichle, R., Liu, Q., Alemohammad, S., Gentine, P., Aida, K., Asanuma, J., Bircher, S.,
786 Caldwell, T., & Colliander, A. (2018). Estimating surface soil moisture from SMAP observations
787 using a Neural Network technique. *Remote Sensing of Environment, 204*, 43-59.
788 Konings, A.G., & Gentine, P. (2017). Global variations in ecosystem ‐ scale isohydricity. *Global change*
789 *biology, 23*, 891-905.
790 Konings, A.G., Piles, M., Das, N., & Entekhabi, D. (2017). L-band vegetation optical depth and effective
791 scattering albedo estimation from SMAP. *Remote Sensing of Environment, 198*, 460-470.
792 Koster, R.D., Dirmeyer, P.A., Guo, Z., Bonan, G., Chan, E., Cox, P., Gordon, C., Kanae, S., Kowalczyk,
793 E., & Lawrence, D. (2004). Regions of strong coupling between soil moisture and precipitation.
794 *Science, 305*, 1138-1140.
795 Kurum, M. (2013). Quantifying scattering albedo in microwave emission of vegetated terrain. *Remote*
796 *Sensing of Environment, 129*, 66-74.
797 Laiolo, P., Gabellani, S., Campo, L., Silvestro, F., Delogu, F., Rudari, R., Pulvirenti, L., Boni, G., Fascetti,
798 F., & Pierdicca, N. (2016). Impact of different satellite soil moisture products on the predictions of a
799 continuous distributed hydrological model. *International journal of applied earth observation and*
800 *geoinformation, 48*, 131-145.

Larson, K.M., Small, E.E., Gutmann, E.D., Bilich, A.L., Braun, J.J., & Zavorotny, V.U. (2008). Use of GPS receivers as a soil moisture network for water cycle studies. *Geophysical Research Letters, 35*

Lawrence, H., Wigneron, J.-P., Demontoux, F., Mialon, A., & Kerr, Y.H. (2013). Evaluating the semiempirical H-Q model used to calculate the L-Band emissivity of a rough bare soil. *IEEE transactions on Geoscience and remote sensing, 51*, 4075-4084.

Lawrence, H., Wigneron, J.-P., Richaume, P., Novello, N., Grant, J., Mialon, A., Al Bitar, A., Merlin, O., Guyon, D., & Leroux, D. (2014). Comparison between SMOS Vegetation Optical Depth products and MODIS vegetation indices over crop zones of the USA. *Remote Sensing of Environment, 140*, 396-406.

Lebel, T., Cappelaere, B., Galle, S., Hanan, N., Kergoat, L., Levis, S., Vieux, B., Descroix, L., Gosset, M., & Mougin, E. (2009). AMMA-CATCH studies in the Sahelian region of West-Africa: an overview. *Journal of Hydrology, 375*, 3-13.

Lemmetyinen, J., Schwank, M., Rautiainen, K., Kontu, A., Parkkinen, T., Mätzler, C., Wiesmann, A., Wegmüller, U., Derksen, C., & Toose, P. (2016). Snow density and ground permittivity retrieved from L-band radiometry: Application to experimental data. *Remote Sensing of Environment, 180*, 377-391.

Liu, Y.Y., Van Dijk, A.I., De Jeu, R.A., Canadell, J.G., McCabe, M.F., Evans, J.P., & Wang, G. (2015). Recent reversal in loss of global terrestrial biomass. *Nature Climate Change, 5*, 470.

Mätzler, C. (1998). Improved Born approximation for scattering of radiation in a granular medium. *Journal of Applied Physics, 83*, 6111-6117.

Mätzler, C. (2000). *Radiative Transfer Models for Microwave Radiometry: Final Report; COST Action 712: Application of Microwave Radiometry to Atmospheric Research and Monitoring-Project 1: Development of Radiative Transfer Models*. Office for Office Publ. of the Europ. Communities.

Mo, T., Choudhury, B., Schmugge, T., Wang, J., & Jackson, T. (1982). A model for microwave emission from vegetation-covered fields. *Journal of Geophysical Research: Oceans, 87*, 11229-11237.

Moghaddam, M., Entekhabi, D., Goykhman, Y., Li, K., Liu, M., Mahajan, A., Nayyar, A., Shuman, D., & Teneketzis, D. (2010). A wireless soil moisture smart sensor web using physics-based optimal control: Concept and initial demonstrations. *IEEE Journal of Selected Topics in Applied Earth Observations and Remote Sensing, 3*, 522-535.

Naderpour, R., & Schwank, M. (2018). Snow wetness retrieved from L-band radiometry. *Remote Sensing, 10*, 359.

Naderpour, R., Schwank, M., & Mätzler, C. (2017). Davos-laret remote sensing field laboratory: 2016/2017 winter season L-band measurements data-processing and analysis. *Remote Sensing, 9*, 1185.

O'Neill, P., Chan, S., Njoku, E., Jackson, T., & Bindlish, R. (2015). Algorithm Theoretical Basis Document (ATBD): L2/3_SM_P. *Initial Release, 3*

Parrens, M., Wigneron, J.-P., Richaume, P., Mialon, A., Al Bitar, A., Fernandez-Moran, R., Al-Yaari, A., & Kerr, Y.H. (2016). Global-scale surface roughness effects at L-band as estimated from SMOS observations. *Remote Sensing of Environment, 181*, 122-136.

Quets, J., De Lannoy, G.J.M., Al Yaari, A., Chan, S., Cosh, M.H., Gruber, A., Reichle, R.H., Schalie, R.V.d., & Wigneron, J.P. (in press). Uncertainty in Soil Moisture Retrievals: an Ensemble Approach using SMOS L-Band Microwave Data. *Remote Sensing of Environment*

Rautiainen, K., Lemmetyinen, J., Pulliainen, J., Vehvilainen, J., Drusch, M., Kontu, A., Kainulainen, J., & Seppanen, J. (2012). L-band radiometer observations of soil processes in boreal and subarctic environments. *IEEE transactions on Geoscience and remote sensing, 50*, 1483-1497.

Rautiainen, K., Lemmetyinen, J., Schwank, M., Kontu, A., Ménard, C.B., Mätzler, C., Drusch, M., Wiesmann, A., Ikonen, J., & Pulliainen, J. (2014). Detection of soil freezing from L-band passive microwave observations. *Remote Sensing of Environment, 147*, 206-218.

Rodríguez-Fernández, N.J., Mialon, A., Mermoz, S., Bouvet, A., Richaume, P., Al Bitar, A., Al-Yaari, A., Brandt, M., Kaminski, T., & Le Toan, T. (2018). An evaluation of SMOS L-band vegetation optical

depth (L-VOD) data sets: high sensitivity of L-VOD to above-ground biomass in Africa. *Biogeosciences, 15*, 4627-4645.
Roy, S.K., Rowlandson, T.L., Berg, A.A., Champagne, C., & Adams, J.R. (2016). Impact of sub-pixel heterogeneity on modelled brightness temperature for an agricultural region. *International journal of applied earth observation and geoinformation, 45*, 212-220.
Saatchi, S.S., Harris, N.L., Brown, S., Lefsky, M., Mitchard, E.T., Salas, W., Zutta, B.R., Buermann, W., Lewis, S.L., & Hagen, S. (2011). Benchmark map of forest carbon stocks in tropical regions across three continents. *Proceedings of the national academy of sciences, 108*, 9899-9904.
Sanchez, N., Martínez-Fernández, J., Scaini, A., & Perez-Gutierrez, C. (2012). Validation of the SMOS L2 soil moisture data in the REMEDHUS network (Spain). *IEEE transactions on Geoscience and remote sensing, 50*, 1602-1611.
Schaefer, G.L., Cosh, M.H., & Jackson, T.J. (2007). The USDA natural resources conservation service soil climate analysis network (SCAN). *Journal of Atmospheric and Oceanic Technology, 24*, 2073-2077.
Schwank, M., Mätzler, C., Wiesmann, A., Wegmüller, U., Pulliainen, J., Lemmetyinen, J., Rautiainen, K., Derksen, C., Toose, P., & Drusch, M. (2015). Snow density and ground permittivity retrieved from L-band radiometry: A synthetic analysis. *IEEE Journal of Selected Topics in Applied Earth Observations and Remote Sensing, 8*, 3833-3845.
Schwank, M., & Naderpour, R. (2018). Snow density and ground permittivity retrieved from L-band radiometry: Melting effects. *Remote Sensing, 10*, 354.
Schwank, M., Naderpour, R., & Mätzler, C. (2018). "Tau-Omega"-and Two-Stream Emission Models Used for Passive L-Band Retrievals: Application to Close-Range Measurements over a Forest. *Remote Sensing, 10*, 1868.
Schwank, M., Li, X., Kerr, Y., Naderpour, R., Mätzler, C., Wigneron, J.-P. (2019). "Tau-Omega"-and Two-Stream Emission Models applied to Close-Range and SMOS Measurements. In, *IGARSS 2019-2019 IEEE International Geoscience and Remote Sensing Symposium*: IEEE.
Serreze, M.C., Clark, M.P., & Frei, A. (2001). Characteristics of large snowfall events in the montane western United States as examined using snowpack telemetry (SNOTEL) data. *Water Resources Research, 37*, 675-688.
Smith, A., Walker, J.P., Western, A.W., Young, R., Ellett, K., Pipunic, R., Grayson, R., Siriwardena, L., Chiew, F., & Richter, H. (2012). The Murrumbidgee soil moisture monitoring network data set. *Water Resources Research, 48.*
Taylor, C.M., Gounou, A., Guichard, F., Harris, P.P., Ellis, R.J., Couvreux, F., & De Kauwe, M. (2011). Frequency of Sahelian storm initiation enhanced over mesoscale soil-moisture patterns. Nature Geoscience, 4, 430.
Tian, F., Wigneron, J.-P., Ciais, P., Chave, J., Ogée, J., Peñuelas, J., Ræbild, A., Domec, J.-C., Tong, X., & Brandt, M. (2018). Coupling of ecosystem-scale plant water storage and leaf phenology observed by satellite. *Nature ecology & evolution, 2*, 1428.
Tuttle, S., & Salvucci, G. (2016). Empirical evidence of contrasting soil moisture–precipitation feedbacks across the United States. *Science, 352*, 825-828.
Ulaby, F.T., Aslam, A., & Dobson, M.C. (1982). Effects of vegetation cover on the radar sensitivity to soil moisture. *IEEE transactions on Geoscience and remote sensing*, 476-481.
Wagner, W., Blöschl, G., Pampaloni, P., Calvet, J.-C., Bizzarri, B., Wigneron, J.-P., & Kerr, Y. (2007). Operational readiness of microwave remote sensing of soil moisture for hydrologic applications. *Hydrology Research, 38*, 1-20.
Wang, J., & Choudhury, B. (1981). Remote sensing of soil moisture content, over bare field at 1.4 GHz frequency. *Journal of Geophysical Research: Oceans, 86*, 5277-5282.
Wiesmann, A., & Mätzler, C. (1999). Microwave emission model of layered snowpacks. *Remote Sensing of Environment, 70*, 307-316.
Wigneron, J.-P., Jackson, T., O'Neill, P., De Lannoy, G., De Rosnay, P., Walker, J., Ferrazzoli, P., Mironov, V., Bircher, S., & Grant, J. (2017). Modelling the passive microwave signature from land

surfaces: A review of recent results and application to the L-band SMOS & SMAP soil moisture retrieval algorithms. *Remote Sensing of Environment, 192*, 238-262.

Wigneron, J.-P., Kerr, Y., Waldteufel, P., Saleh, K., Escorihuela, M.-J., Richaume, P., Ferrazzoli, P., De Rosnay, P., Gurney, R., & Calvet, J.-C. (2007). L-band microwave emission of the biosphere (L-MEB) model: Description and calibration against experimental data sets over crop fields. *Remote Sensing of Environment, 107*, 639-655.

Wigneron, J.-P., Laguerre, L., & Kerr, Y.H. (2001). A simple parameterization of the L-band microwave emission from rough agricultural soils. *IEEE transactions on Geoscience and remote sensing, 39*, 1697-1707.

Wigneron, J.-P., Mialon, A., De Lannoy, G., Fernandez-Moran, R., Al-Yaari, A., Ebrahimi, M., Rodriguez-Fernandez, N., Kerr, Y., Quets, J., & Pellarin, T. (2018). SMOS-IC: Current status and overview of soil moisture and VOD applications. In, *IGARSS 2018-2018 IEEE International Geoscience and Remote Sensing Symposium* (pp. 1451-1453): IEEE.

Wigneron, J.-P., Waldteufel, P., Chanzy, A., Calvet, J.-C., & Kerr, Y. (2000). Two-dimensional microwave interferometer retrieval capabilities over land surfaces (SMOS mission). *Remote Sensing of Environment, 73*, 270-282.